Improving Suturing Skills for Surgical Residents and Advancing Prosthesis Control for Amputees

by

Daniel Catalin Ursu

A dissertation submitted in partial fulfillment
of the requirements for the degree of
Doctor of Philosophy
(Mechanical Engineering)
in the University of Michigan
2016

Doctoral Committee:

        Associate Professor R. Brent Gillespie, Chair
        Assistant Professor Cynthia A. Chestek
        Associate Professor Kathleen H. Sienko
        Research Associate Professor Melanie G. Urbanchek

2016

DEDICATION

To all of you who have made possible, this incredible journey.

A C K N O W L E D G M E N T S

I would like to express my appreciation and gratitude to a number of individuals who have contributed to the different phases of my development as an engineer and research scientist. First and foremost, I would like to express my deepest gratitude to Professor R. Brent Gillespie for the intellectual suggestions, helpful criticisms, and valuable support provided at all hours of the day during my doctoral studies at the University of Michigan. Brent, thank you for your patience, guidance, and mentorship.

Next, it is imperative that I thank Professor Melanie Urbanchek for offering me the privilege of contributing research in her laboratory. Mel, you were instrumental in changing my mindset from that of the engineer into a scientist. Thank you for encouraging me to succinctly define my research proposals and hypotheses and for letting me learn from your love for animals. The past three years have been an honor.

I also would like to sincerely acknowledge the contributions made by Professors Kathleen Sienko and Cynthia Chestek. Because of the two of you, this thesis reflects a better understanding of the space I occupy in my research field.

Finally, my family has shown tremendous support over the years. I am very grateful to you for the unconditional support you have always provided. Your love and encouragement have turned this dream into reality.

TABLE OF CONTENTS

LIST OF FIGURES

LIST OF TABLES

LIST OF ABBREVIATIONS

CMAP compound muscle action potential

CNS central nervous system

DOF degree of freedom

EDL extensor digitorum longus muscle

EMG electromyography

sEMG surface electromyography

FE finite element

pNG peripheral neurography

PSD power spectral density

RPNI Regenerative Peripheral Nerve Interface

RMS root mean square value

SIS small intestinal submucosa

TMR Targeted Muscle Reinnervation

ABSTRACT

Proper suturing technique is one of the most important skills a surgical resident should acquire during training. However, current methods for teaching suturing technique rely only on subjective performance evaluations. An instrumented training apparatus for abdominal closure could be used to define objective assessments that are directly related to the quality of the closure. I identify a synthetic material that models abdominal fascia using porcine and cadaveric data and design a means to mount the material so that it mimics the challenges of abdominal closure. Digital images are used to quantify deformations in the material and provide real-time objective measures regarding the effect of suture placement and tension on deformations remaining in the abdominal tissue after closure. In parallel, I develop a finite element model of abdominal fascia and its closure with suture to deduce stresses in the material and forces in the sutures from the measured deformations. I find that despite uniform suture spacing, the forces in the suture are not evenly distributed along the closure. These findings further motivate the development of a surgical learning tool that objectively relays information about both suture *placement* and *tension*.

In a second body of work, I address the development of a novel interface between the peripheral nervous system of an amputee and a motorized prosthetic device. Conventional myoelectric control cannot produce a sufficient number of independent signals for actuation of modern multiple degree of freedom (DOF) upper limb prostheses. A compact construct involving grafted muscle surgically prepared at the end of a transected peripheral nerve is envisioned for transducing a nervous signal with fine specificity and sensitivity. Up to 20 such constructs can be prepared in a human arm, and an epimysial electrode on each construct can then be used to relay signals encoding 20 independent channels of motor intent. I develop a means of evaluating this construct in

awake rats, and demonstrate that the transduced signals suffer minimal crosstalk and are correlated with gait kinematics. A decoder is also able to reconstruct data produced by motion tracking, and I show that adjacent constructs placed proximal to one another provide the same signals as anatomically intact muscle-nerve antagonist-pair analogs. The correlation between the signals transduced, the walking kinematics and analogous out of phase activation obtained from adjacent constructs indicates that this technology holds promise for translation to humans.

CHAPTER 1

Introduction

1.1 Foreword: A Matter of Definition

Typical mindsets in medical science and engineering are not always compatible. Particularly telling in this regard is the distinction between the way a medical scientist and engineer would go about modeling a given system. Speaking broadly, the kind of model that the medical scientist turns to is an empirical model, whereas the initial kind of model the engineer turns to is one based on first principles. The empirical model is built on observed data, i.e. it is fundamentally data-driven. A model built on first principles also seeks to describe data, but produces or predicts that data (derives its function) based on axioms. At the core of a first principles model is a reference to mechanics and physics. Mathematical expressions for this reference are set up according to laws of physics and mechanics. The behavior of the model (under simulation or computation or analysis) is then governed by these principles. The behavior of the empirical model, on the other hand, is governed by formulas chosen so that behavior (maps from inputs to outputs) is chosen as the simplest possible required to best fit the data.

The different approaches to system modelling adopted by the medical and engineering communities may have influenced the rather distinct definitions of a *system* adopted by each. A medical definition of *system* is: "a school or method of practice based on a specific set of principles" or "a set or series of interconnected or interdependent parts or entities (objects, organs, or organisms) that act together in a common purpose or produce results impossible by action of one alone" [1]. For the engineer, a *system* is an entity which interacts with other variables in the environment, and importantly, produces observable outputs. These variables may be possibly known and measurable inputs, as well as disturbances whose effects remain to be characterized. The outputs are then a function of these inputs and disturbances, as well as the internal workings (i.e. states) of the system [2]. And modeling how such a *system* would perform under different environmental conditions requires that the model be driven by quantifiable physical and mechanical phenomena.

There is good reason for a medical scientist to shy away from a first principles model. Living

organisms are so complex that describing them based on laws of physics is usually an exercise in futility. Hence, medical scientists are most often observing behaviors (perhaps while simultaneously manipulating experimental conditions) and exploring cause and effect. The chief interest of the medical scientist lies in determining relationships for the purpose of understanding. Data reduction is the process and cause and effect are the basic measurable outcomes of the behavior of a living system under study. On the other hand, the engineering mindset is usually characterized by establishing the building blocks that make something work. Modeling is the engineer's chief activity, and models are not only used to describe, but also to build, to extrapolate, to put to use, to integrate the known into something bigger. Engineers approach most problems they face with a toolbox outfitted with first principles and mathematical models.

As someone dedicated to a research career which spans both the medical and engineering disciplines, my goal is to bring engineering tools and principles to bear on problems of translation in medicine. I am thus very interested in finding an appropriate balance between reliance on empirical data and a need to seek out first principles with which to characterize a system's behavior. This balance is always guided by the end-goals of the translational research objectives which captivate my attention. As such, at times empirical models are appropriate; and sometimes first principles models. For if discovery is the mantra of science, my tenet is also that of the tinkerer: "combine science and technology know-how with infectious enthusiasm for creating something and putting it to work."

There are two rather distinct bodies of work that will be documented in this thesis, both of which have been guided by a balance between first principles and empirical approaches toward system modelling. Examples of first principles appear especially in Chapter 2, which addresses surgical skill training and utilizes a finite element model of tissue mechanics to investigate the suture tension required for a simulated abdominal closure. An example of empirical model application, a mathematical decoder built to map the function of a novel prosthetic interface to the peripheral nervous system, is addressed in Chapter 3. Moreover, Chapter 4 is a further example of the broad medical definition for *system* governing my research in human-prosthetic interface development; the goal of this work is to describe the dependence of signals on various environmental factors and compare them to a known neuromuscular output, rather than understanding all details of the complex underlying neurophysiology.

1.1.1 Chapter 2: Training Surgical Skills

The surgical resident in training is a system in both senses of the medical definition. It is, first, a living organism (though the fatigue accumulated from the long working hours may make him or her feel otherwise)! But arguably, when performing an abdominal closure with suture, he or she

is also the product of a school or method of practice based on a specific set of principles. These principles dictate that a successful abdominal closure requires that wound edges be approximated with equidistantly placed throws of suture. Competency is evaluated in a subjective manner, in part because of the lack of adequate assessment tools required to quantify the optimal tension required in an abdominal closure.

Yet training residents to appropriately place and tension suture while performing an abdominal fascia closure is an important means to minimize post-surgical complications such as incisional hernia [3]. To address this objective, I have developed a computational model of abdominal fascia that can be subjected to treatments that simulate a closure with suture, and a physical model that can be closed with real suture. Experimental results involving animal and cadaveric abdominal fascia informed the selection of material properties and materials for the computational and physical models. The physical model is used to verify the computational model and subsequently the computational model is used to interpret displacement fields. The physical model is also envisioned as a trainer for surgical residents, with the ability to provide automated performance feedback regarding suture placement and tension.

The development of complex surgical procedures coupled with more stringent regulations on medical education has bolstered the need for developing reality-based surgical simulators for medical training. Regulations on the maximum working hours permitted for medical residents limits the amount of time available to practice common surgical tasks such as needle insertion, suturing, cutting, dissecting and electrocauterizing tissue.

Surgical simulators are commonly grouped into three categories: anatomy, physics, and physiology based simulators [4]. Anatomy simulators do not incorporate components such as tissue deformations, and are instead based on the geometrical structure of the anatomy involved in the simulation task. Surgical trainers of this type have been mainly used for intubation or endoscopic procedures, where little interaction with the environment is required, and visualization of the simulation task is deemed sufficient [5]. Physics and physiology based simulators attempt to replicate a surgical procedure as accurately as possible, and are employed where visualization of the surgical task by itself is deemed insufficient. These simulators require precise characterization of the interactions between surgical instruments and soft tissue, and attempt to model the material response of the tissue as accurately as possible.

Both empirical (data driven) and constitutive (phenomenological mathematical equations used to describe the relationships between physical quantities) models have been successfully employed to computationally render the behavior of tissue in virtual environments. For example, modeling needle insertion into soft tissue has been developed for surgical training and planning simulators, as well as for robotic needle steering. Empirical models [6], and fracture mechanics analytical models [7] have been used to predict needle force and its relation to either global deformation, the

3

tissue geometry, boundary conditions surrounding the tissue, or insertion velocity. These models are based on detailed studies of biological samples, which have shown that soft tissue behaves in a nonlinear fashion under different loading conditions [8–11].

Finite element (FE) models are of particular interest in virtual surgical simulation applications due to their increased accuracy and continuous representation of volumetric tissue deformation. The improvement in realistic deformation however, comes at the cost of computational complexity, [12–14], which requires either significant computational resources [15] or a restriction of the tool paths by which the user may interact with the virtual tissue in real time [16].

To overcome the computational complexity required to model the behavior of soft tissue in a virtual environment, yet still take advantage of the accurate information regarding tissue dynamics that can be provided by an FE model, the work described here attempts to develop a physical model of abdominal fascia closure. A thin neoprene sheet is employed as an abdominal fascia substitute material, following mechano-elastic and surgical tool interaction validation studies performed on porcine and human cadaver abdominal tissues, similar in scope to assessments performed by SynDaver™ Labs in designing commercial high fidelity synthetic tissue models employed in medical simulation and training [17]. The sheet is marked with a dotted grid, which deforms as the user stretches, incises then closes the material with suture. In parallel, an FE model of an analogous virtual neoprene sheet is developed. This computational model is capable of informing the forces required to close an incision in the virtual neoprene with suture as a function of either suture placement, material deformation, or incision edge apposition. Both physical and computational models employ a similarly spaced dotted grid, allowing the comparison of one model to another via the superposition of the dotted grids using digital image correlation techniques.

Specifically, to better understand the mechanics underlying abdominal fascia closure and develop a surgical trainer to aid in the appropriate placement and tensioning of suture, I contribute the following:

- a new model of abdominal closure based on physical (solid mechanics) principles,

- a quantification of the suture tension required to bring incised edges into apposition for a variety of suture locations,

- a demonstration that suture tension and placement are separate entities contributing to the proper closure of an incised abdomen,

- use of a solid mechanics model to support a heretofore unexplored anecdotal claim that more tension is required to hold the middle part of the incision edges together than the outer edges of an abdominal closure.

4

1.1.2   Chapter 3: In Vivo Function of a Neuromuscular Interface

Considerable scientific and technological efforts have been devoted to develop interfaces that link the human nervous system to robotic devices with the aim of restoring motor and sensory functions in amputees and persons with neurological impairment.

The best location to detect action and sensation intuitively is undoubtedly the brain. Brain machine interfaces have the potential to thus optimally control and receive information from a computerized prosthetic device, by acquiring salient information at its point of origin. Significant research efforts have demonstrated [18], or are currently underway [19, 20] to develop biocompatible electrode arrays capable of interfacing with the cortex.

As neural information travels down through the body to sensory and motor end-organs, peripheral neurography (pNG) can, via the use of specialized electrodes, send and receive signals at the neurofascicular level. Previous studies using cuff electrodes placed on whole peripheral nerves [21], cuff electrodes interfacing with individual nerve fascicles [22, 23], and intra-axonal electrodes [24] have demonstrated the possibility to stimulate and record neural signals from peripheral nervous tissue. However, mechanically induced neural injury at the electrode-nerve interface and biocompatibility issues leading to scar formation on neural tissue are problems which limit the long term use of such interfaces [25], and must be addressed prior to FDA approval [26].

Distally, neural motor signals innervate muscle. A consequence of this innervation is the transduction and amplification of these signals via musculature into electromyography (EMG). By indirectly engaging the peripheral nervous system, intramuscular and surface EMG can transmit muscle-specific efferent information to a prosthetic device, and EMG electrodes are the current state of the art for controlling upper or lower limb prosthetic devices [27]. A notable peripheral nerve interface that uses transduced neural signals is Targeted Muscle Reinnervation (TMR), which is based on a nerve transfer to denervated but otherwise intact residual muscle. For certain proximal amputee populations, TMR is a surgical intervention that enables the transduction, using surface EMG on alternate muscles, of nerve signals that previously produced actions in the amputated limb. Following the procedure, the transferred nerve endings evolve functioning synapses within the new muscle. Patients can contract these newly innervated muscle regions by attempting natural intended volitional movement. The muscle contractions have been successfully detected by surface EMG electrodes, creating additional sites of control for a myoelectric prosthesis and allowing natural-feeling operation of prosthetic limbs [28, 29]. TMR has also been combined with pattern recognition technology to provide above-elbow amputees control of multiple prosthetic functions simultaneously [30]. While TMR surgery has been performed successfully in select patients, difficulties related to prosthetic control accuracy and stability remain significant obstacles. Notably, challenges include difficulty with separating surface EMG signals, especially during co-activation of muscles within the residual limb, which generates signal interference [31].

Paul Cederna and Melanie Urbanchek of the Neuromuscular Laboratory at the University of Michigan have developed the Regenerative Peripheral Nerve Interface (RPNI), which, like TMR, is envisioned as an interface between an amputee and a motorized prosthesis. The RPNI is based on a reinnervated free muscle graft equipped with an intramuscular or epimysial electrode. While TMR is based on moving the nerve to muscle, the RPNI is based on moving muscle to nerve. The RPNI is a very small surgically prepared construct, about 2 cm long and 1 cm in diameter. Up to 20 RPNI could potentially be prepared in the residual arm of an amputee, thus creating 20 independent signal channels, each of which could be mapped to a degree of freedom of a motorized prosthesis.

Previously, the viability of rat RPNI constructs had been demonstrated using evoked responses. This chapter addresses the next critical step for assessment of the RPNI as a control modality for prosthetic devices; in vivo characterization of RPNI function during a walking task in awake rats. Two RPNIs were created in each of two rats by grafting portions of free muscle to the ends of divided peripheral nerves (peroneal in the left and tibial in the right hind limb) and placing bipolar electrodes on the graft surface. Post surgical healing, I examined in vivo EMG signal activity and compared these signals to muscular EMG signals recorded from autologous muscles in two rats serving as controls. An additional group of two rats in which the autologous muscles were denervated served to quantify cross-talk in the electrode recordings. Recordings were made while rats walked on a treadmill and a motion capture system tracked the hind limbs. Amplitude and periodicity of signals relative to gait were quantified, correlation between EMG and motion recording were assessed, and a decoder was trained to predict joint motion. This work demonstrated that raw RPNI signals were active during walking and quiet during standing, with amplitudes similar to Controls. Signal contamination from muscles adjacent to the RPNI was minimal, as demonstrated by the low amplitude signals obtained from the Denervated group. Moreover, RPNI signals were periodic and entrained with gait. A decoder predicted bilateral ankle motion with predictive power similar to the Control group.

Specifically, to demonstrate the feasibility of the RPNI for encoding neural activation patterns associated with gait, I contribute the following:

- the first in vivo evaluation of RPNI Function,

- a demonstration that RPNI signals possess the same large order of magnitude as Controls,

- a demonstration that RPNI signals retain constant amplitude over time (of evaluation),

- validation that RPNI signals not affected by motion artifact or activity from adjacent muscles,

- evidence that RPNI signals are periodic, and entrained with the observed gait during a walking task.

1.1.3   Chapter 4: In Vivo Function of Adjacent Neuromuscular Interfaces

The small size of the RPNI, and the ability to control the source of reinnervation inherent to the construct's design render the placement of multiple such constructs in proximity to one another an exciting possibility. To evaluate whether adjacent RPNIs can deliver intuitive independent control signals to different DOF of a prosthetic device, this chapter investigates whether adjacent RPNIs are capable of producing independent signals in a rat model. Two RPNIs neurotized with peripheral nerves known to produce agonist / antagonist signals were surgically created in the left hind limb of rats. The first construct was neurotized by a foot dorsi-flexor (peroneal) nerve and the second neurotized by a foot plantar-flexor (tibial) nerve fascicle. Dual-RPNI function was contrasted with signals obtained from Control rats, which had electrodes implanted onto the soleus and extensor digitorum longus muscle (EDL) muscles in the left hind limb. Amplitude and periodicity of all signals relative to the gait period were quantified during a treadmill walking task. To facilitate comparisons across groups, processed EMG signals were expressed as a percent of total stepping cycle activity for each stance and swing gait phase.

Independence between peroneal nerve and tibial nerve activations and quiescent signals were assessed by comparing Control group and Dual-RPNI group differences during stance and swing, respectively. This analysis showed that EMG activity for Control and Dual-RPNI rats display similar alternating patterns of activation coinciding with stance and swing. As expected, signals from both Control and Dual-RPNI rats were quiet during stance. Since these differences were of similar magnitude to those found for the Control group it follows that signals obtained from adjacently placed RPNIs is independent during both stance and swing.

Specifically, to validate that adjacent RPNIs neurotized with agonist/antagonist nerves activate independently during voluntary walking, with signal activity patterns similar to Control, I contribute the following:

- a demonstration that RPNI constructs reinnervated with fascicles of peripheral nerves are viable, provide same amplitude as whole peripheral nerve enervated constructs,

- a demonstration that RPNIs constructed with muscle isografts of different innervation origin are viable (i.e. source of muscle isograft does not affect RPNI function)

- evidence that RPNIs constructed with nerves providing antagonist muscle activation demonstrate activity profiles similar to analogous antagonist muscle pairs in Controls during stance

7

and swing phases of gait.

1.1.4 Outline

In the chapters that follow I describe how I have brought a systems modeling and analysis viewpoint to these two domains. In particular, I have applied signal and image processing, correlation analyses, biomechanical models, and solid mechanics models in the fields of medical education and prosthetics research in order to further the development of the next generation of surgical skill training, and human-prosthetic interfaces.

CHAPTER 2

An Abdominal Fascia Closure Simulator Supported by a Computational Model

2.1 Introduction

Incisional ventral hernia is the most common complication in general surgery [32,33]. Laparotomy incisions fail to heal 11% of the time and subsequently progress to incisional hernia [34]. This high rate of surgical wound failure results in 200,000 re-operations each year in the United States, at an estimated cost of $2.5 billion [35]. With 4 million laparotomies performed each year in the US, the true incidence of laparotomy wound failure and incisional hernia formation approaches 400,000 cases per year. While biologic and patient factors certainly contribute to the development of incisional hernia, the technique and clinical experience of the surgeon also has a quantifiable impact on the risk of incisional hernia [36, 37]. For example, the risk of incisional hernia formation has been linked to whether the abdominal closure was performed by a resident or an attending surgeon [3], with one study showing hernia development rates of 13.2% for closures performed by surgical residents as compared to 4.3% for attending surgeons [38].

Recommendations are available regarding the placement of suture for abdominal closure, based on multi-center clinical trials [3, 36, 37, 39–41]. In particular, a running closure is recommended, using non-absorbable suture with a 1 cm bite and a 1 cm travel, as illustrated in Figure 2.1. Recommendations regarding suture tension are much more subjective, and generally follow the dictum "approximate, but don't strangulate," i.e. bring the wound edges together, but not so tight as to induce ischemia. Neither non-approximated wound edges nor ischemic tissue can be expected to heal. However, the only recommendation accompanied by clinical evidence pertaining to setting tension is given in terms of the ratio between the length of suture used and the wound length. A suture length to wound length ratio of 4:1 is recommended alongside 1 cm bite and 1 cm travel [42]. But this directive is at best an indirect means of controlling tension.

A direct means for estimating tension in the suture or stresses in the tissue are unfortunately not available—neither based on observations made during the procedure, nor once the closure is

complete. Further complicating matters, setting tension during an abdominal closure involves a team of two surgeons, one who manipulates needle and tissue and a second who "follows" by holding tension in the suture while the first places the next stitch.
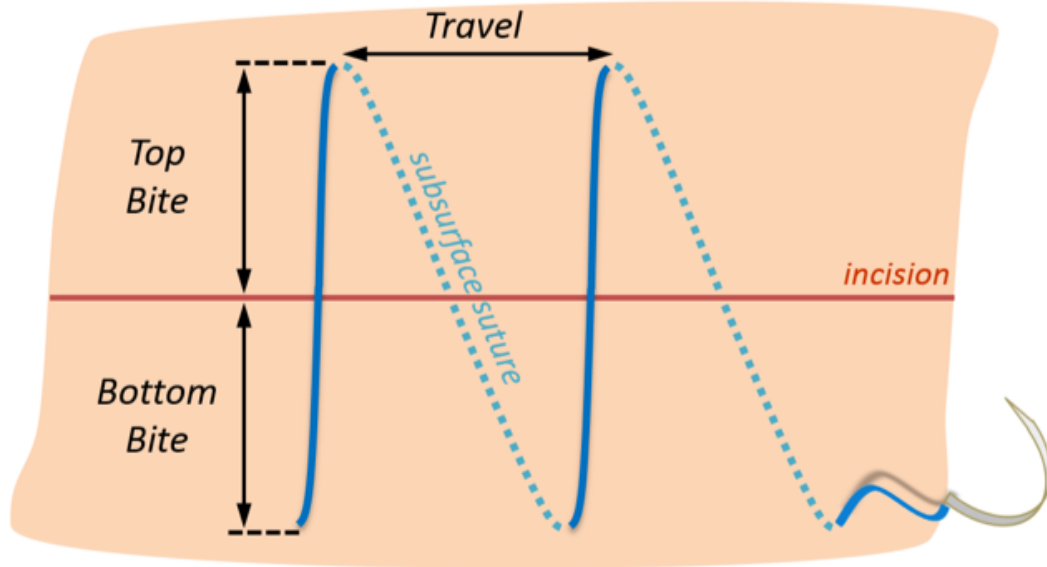
Figure 2.1: Schematic of abdominal fascia closure performed using continuous suture, illustrating bite and travel parameters.

Both the estimation of tension and the development of guidelines for setting tension in the sutures that optimally promote healing could be informed by a model of the mechanics of the tissue and closure. Knowledge of the distribution of forces in the suture along a wound closure would be helpful to delineate optimal tension, as would the distribution of stress in the tissue along the wound edge, and in the neighborhood of the sutures. A model of the tissue mechanics might even function as a possible interim step between current understanding of clinical practice and outcomes, and eventual clinical trials that directly measure suture tension and abdominal stress. Also, a tissue mechanics model could be useful for communicating and training optimal technique to surgeons-in-training; currently objective feedback is not available to residents beyond an observing faculty member's subjective assessment of the trainee's technique.

In this chapter, I present a computational model intended to describe abdominal fascia initially subjected to uniform stress, then incised, and finally closed with suture. I also present a physical model of abdominal fascia that can be subjected to similar treatments and used to verify the com-

putational model. The physical model plays a secondary, but highly relevant role as a trainer of surgical technique for surgical residents. I envision that a computational model could be used to convert measurements made (using image analysis) on the physical model into estimates of suture tension and objective performance feedback for a surgical resident. The physical and computational models might play a useful role in determining optimal closure technique.

The computational model was constructed first, by drawing on the wealth of available results from the field of solid mechanics concerning crack formation and propagation [43–45], as well as tissue mechanics regarding the mathematical modeling of biological tissues [46, 47]. In particular, a linear elastic model was adopted as a starting basis, was subjected to pre-stresses, and then the incision and subsequent closure were simulated via both continuous edge apposition and discrete locations of applied force. I investigated the amount of tension needed to bring the tissue edges in apposition as a function of distance along (travel), and away from (bite) the incision midline.

The physical model/surgical trainer employs a thin sheet of neoprene pre-marked with a grid of dots with 1 cm spacing. This simulated tissue is subjected to a uniform stress, then incised and subsequently sutured closed. A camera placed overhead is used to record an image of the neoprene in three states: (1) stretched, (2) incised, and (3) closed. Image processing is then employed to analyze the displacements within the dotted array under each condition, thereby providing an objective measurement of the deformation in the neoprene sheet when it is stretched, incised, and finally sutured closed. The computational model is used in conjunction with the physical model/surgical trainer to study the effects of suture placement and tension on tissue, and to inform the design of the performance feedback to be given to the resident in training.

In the following, I describe the construction of the computational and physical models of abdominal closure. The physical model is used to validate the computational model and inform proper suture placement and tension. I compare the performance of the physical model and computational model under initial material stretch, incision, and closure. I also use the computational model to demonstrate its promise for the determination of optimal placement and tensioning of suture for abdominal closure.

2.2 Materials and Methods

2.2.1 Experimental Apparatus

A surgical trainer (physical model) was constructed for instructing medical students and surgical residents in the practice of abdominal fascia closure. The design requirements for the trainer included the ability to incorporate an inexpensive, easily replaced sheet of material that would exhibit the following behaviors: 1) mimic the elastic properties of abdominal fascia when stretched

over a frame, 2) produce an opening of similar size and shape when incised with a scalpel, 3) render an appropriate interaction force and feel when punctured and driven through with a needle, and 4) require similar forces applied to suture to pull the incised edges back together (to re-approximate the edges). A means of consistently measuring the deformation of the sheet as it is stretched, incised, then re-approximated was also required.

To meet these design criteria, I constructed a frame using lightweight aluminum struts that could be adjusted for height. The square frame was sized with a width of 350 mm so as to accommodate a 200 mm long incision in the stretched sheet that could be cut and subsequently closed with running suture. Above the platform, a fixed camera holder was devised for the purpose of recording the suture placement along the closure. Where the material was to be held in place on the platform, anchors were installed with a 50 mm spacing. To objectively assess the various states of deformation of the material as it is stretched, incised, then closed, I opted for marking the sheet with a uniform gridded dot pattern of 44 by 27 dots spaced 1 cm apart, and analyzing displacements with image processing. Figure 2.2 depicts the physical model/surgical trainer prototype, first without the sheet, then with a sheet stretched, incised, and closed.

In the following I describe the selection of the abdominal fascia material substitute, along with the means for generating quantitative feedback for a medical student or surgical resident in training. To identify an initial set of candidate materials possessing similar mechanical properties to abdominal fascia, I used a commercial database of materials known as the Cambridge Engineering Selector (CES, Granta Design, Cambridge, UK). I specified a target material behavior using certain mechanical properties of human abdominal fascia available in the literature [48], including Young's Modulus, tensile strength, and maximum tensile strain. I also compared artificial material behavior to the behavior of abdominal fascia of four adult pigs and one human cadaver under various treatments. All animal care and use procedures were conducted in accordance with the National Research Council's *Guide for the Care and Use of Laboratory Animals* (1996) and were approved by the University of Michigan Animal Care and Use Committee.

In detail, the four porcine animals were anesthetized and secured supine on an operating table in a sterile field. The abdominal midline was marked using india ink from the superior xyphoid process to the inferior mons pubis. An 18-22 cm long incision was then made along this guide. Photos were taken before and after the incision was performed, using a ruler to assess the deformation of the abdominal fascia after incision. A similar procedure was undertaken in the cadaver. The photographed incisions were then measured and characterized using MATLAB's Image Processing Toolbox (The MathWorks Inc. Natick, MA).

To ensure an approximate match between the elastic properties of candidate materials and target tissues, I quantified the force required to pull the cut edge of porcine and cadaver preparations back to midline. To perform these measurements, a low friction caliper tool (Mitutoyo, Aurora
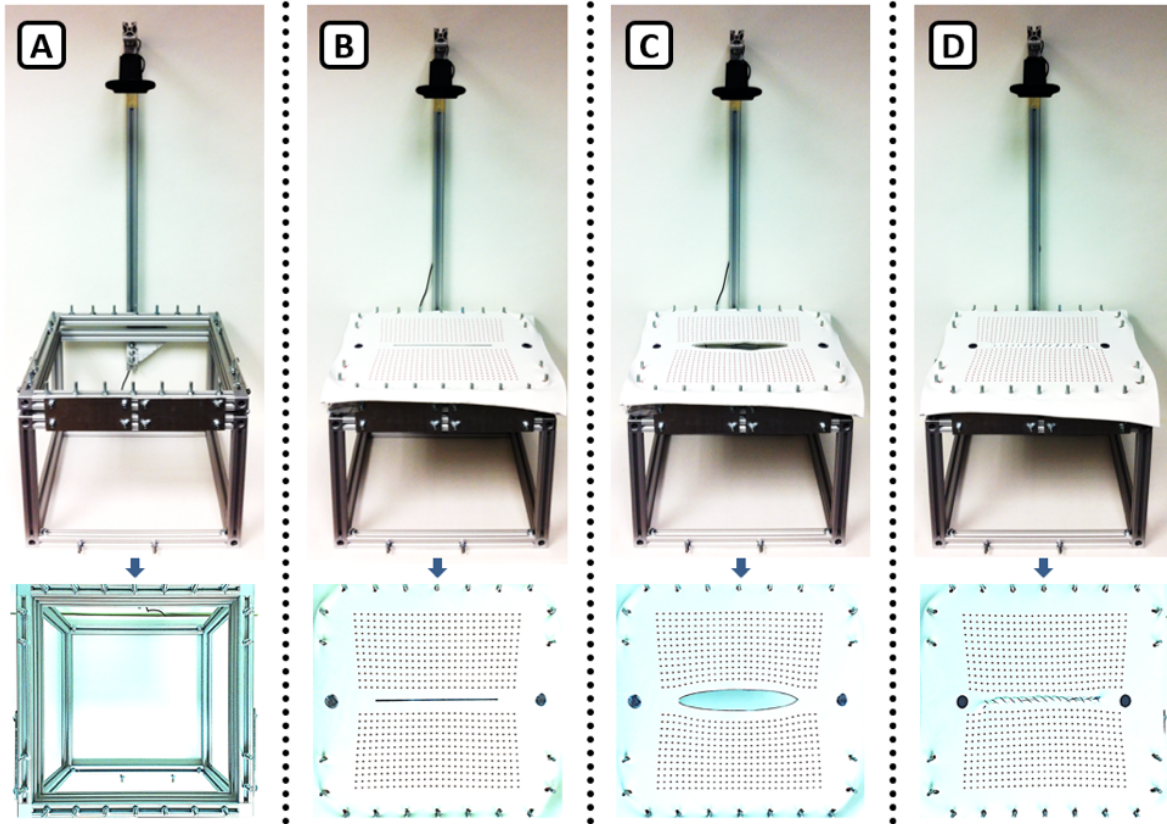
Figure 2.2: (Top) Illustration of simulator prototype platform and (Bottom) view from the overhead camera under four consecutive loading conditions: **A.** Simulator platform frame; **B.** Simulator platform loaded with uncut sheet stretched onto side anchor pegs; **C.** Simulator platform and sheet incised along the midline; and, **D.** Simulator platform with sheet closed using a continuous suture technique.

IL), equipped with a needle driver and a precision extension spring (McMaster-Carr, Elmhurst IL), was manipulated to pull the target fascia tissues and candidate artificial materials to midline in a smooth motion. The tension required to pull to midline was available by multiplying the caliper's displacement readout with the calibrated spring constant (approx. 0.075 N/mm $\pm$ 5%). Figure 2.3 illustrates the force measurement device.

A number of materials in sheet form (silicone elastomers, rubber composites, high density foam sheets, and neoprene) were considered as candidates to simulate the mechanics of fascia tissue. The behavior of each candidate material was objectively and subjectively assessed when stretched over the frame, when incised with a scalpel, when pulled back to midline using forceps, when punctured with a needle, and when the incision was closed with a running suture. Based on these evaluation results, a 400 mm by 400 mm square sheet of neoprene 2 mm thick was selected as the best candidate. An iterative process of stretching, incising, and pulling the material back to

Figure 2.3: A calibrated spring stretched across the jaws of a digital readout calipers enables the determination of tension applied to produce a specified displacement of the incision edge. Force is applied to the proximal caliper jaw by hand and to the distal jaw by the locking needle driver secured to the abdominal fascia.

midline informed the amount of stretch in all directions (10-15 mm per side).

To objectively assess the deformation of neoprene as it was stretched on the simulator platform, incised, then closed with continuous suture, a 27 by 24 grid of dots with 2 mm diameter and 1 cm by 1 cm spacing was inscribed onto the neoprene sheet. The grid pattern was centered about the material's midline, where the incision and subsequent closure were to be performed. To inscribe the red grid pattern on the white neoprene sheets, a commercial screen printer from a local T-shirt printing company that could imprint the sheets in bulk was employed. A camera placed overhead (Model C920, Logitech USA, Fremont, CA) was used to image the neoprene under three conditions: stretched, incised and closed. Image processing was then employed to find the centroids of the dotted grid, and analyze the displacements within the dotted array under each condition, thereby providing an objective measurement of the deformation in the neoprene sheet as it was stretched, incised, then sutured closed.

2.2.2   Computational Model

To better understand the stresses and deformations that can be expected in a thin neoprene sheet acting as a substitute for abdominal fascia, I utilized finite element (FE) modeling software provided by COMSOL Multiphysics (COMSOL, Inc. Burlington, MA). I simulated a sheet of virtual neoprene being loaded, deformed, incised, and closed in the same way the actual neoprene sheet was treated. In detail, the virtual neoprene model was dimensioned precisely as the actual thin neoprene sheet (300 x 300 x 2 mm) and was marked with a dotted grid identical in size, spacing and placement to the actual neoprene. Young's Modulus (0.7 MPa) and Poisson's Ratio

(0.49) were set using values for neoprene available in the database of the Cambridge Engineering Selector. Due to the neoprene sheet's symmetry about its midline, a half-plane model was used. A symmetry constraint about the midline was imposed, while the 200 mm edge of the incision was allowed to deform freely, as per Figure 2.4. The virtual neoprene's outer top edge was stretched 15 mm at its anchor points, while the side edges were stretched 10 mm or 15 mm at the side anchor points according to the placement of the pegs onto which the real neoprene sheet was loaded.
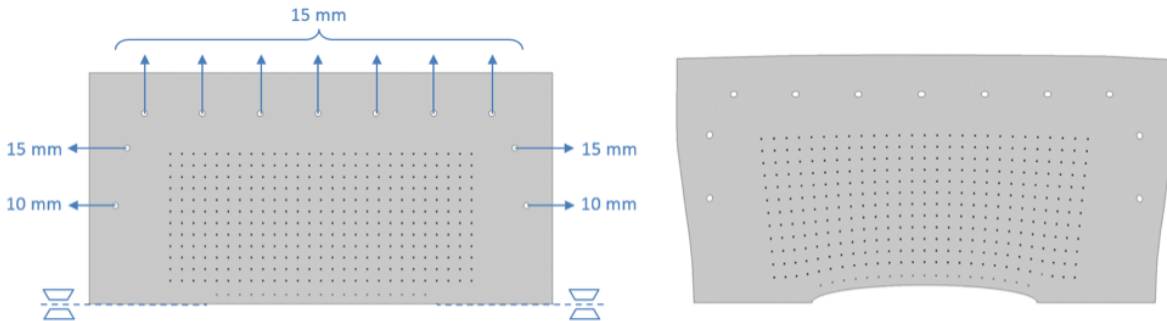
Figure 2.4: Finite Element Model of a virtual neoprene sheet inscribed with a dotted array. On the left, the model's prescribed displacement at each anchoring site is indicated, as well as the symmetry constraint imposed about the midline. The bottom mid-section of the model was allowed to deform freely. On the right, the deformed model is shown, as produced by solving for the constraints in a finite element study.

The resulting deformed and incised virtual neoprene, as well as the stress and strain that developed in the material due to this deformation, were used as initial conditions for subsequent studies in which the crack that developed along the neoprene midline was closed. Closures were simulated using either a continuous force along the crack edge, or tension applied at discrete points along the edge and at various bite locations. The outputs from the computational FE model were compared with analogous experiments performed on the physical model / surgical trainer, to assess agreement between the real and virtual neoprene treatments. Figure 2.5 depicts such a comparison, in which real neoprene and the virtual computational model were analogously stretched at a discrete location to midline, to assess the force needed to hold the neoprene edges together at an individual location.

2.2.3 Data Analysis

Comparisons between incision opening size and shape, and the forces required to pull the incised edges back to midline, were performed between the porcine and cadaveric incised abdomens,
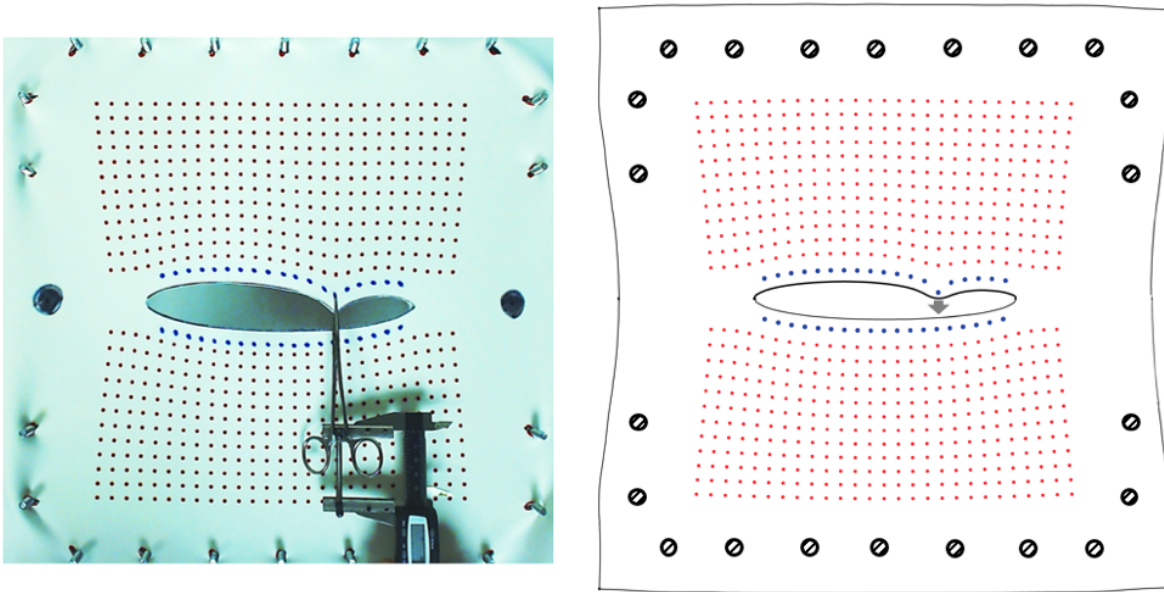
Figure 2.5: Illustration of real neoprene sheet and analogous virtual model being stretched back to midline post incision in a discrete location. The real neoprene sheet stretch is achieved with the modified caliper force measuring tool shown in Figure 2.3.

as well as the computational and physical neoprene models. An additional comparison metric using the dotted grid as a basis was performed between the neoprene material and computational model, as follows: Using image processing, the computational model's virtual neoprene output and real neoprene pictures taken during initial stretching, post-incision, and post-closure with continuous suture were overlaid, using the anchor pegs as reference points. The dotted grid point locations for both the virtual neoprene obtained from the computational model and real neoprene were calculated, and differences between the two grids assessed. The resulting displacement field between the two grids allowed the quantification of the computational model's fidelity.

2.3 Results

2.3.1 Crack Opening

Comparing the gaps produced after incising a single cadaveric and four porcine abdominal fascia samples to the gap produced by incising an actual neoprene sheet revealed that the cadaveric and porcine samples achieved a wider gap than the neoprene, with the cadaveric preparation exhibiting the highest amount of tissue relaxation. However, the virtual neoprene computational model's simulated gap was in good agreement to its analogously treated actual neoprene coun-

terpart, and both aligned acceptably well with the shape and relative size of the gap achieved in the live porcine model. Figure 2.6 shows the incision gap profile calculated for the virtual neoprene computational FE model, and found for the actual neoprene sheet, cadaver, and four porcine samples, using image processing of the pre- and post-incised abdomen.
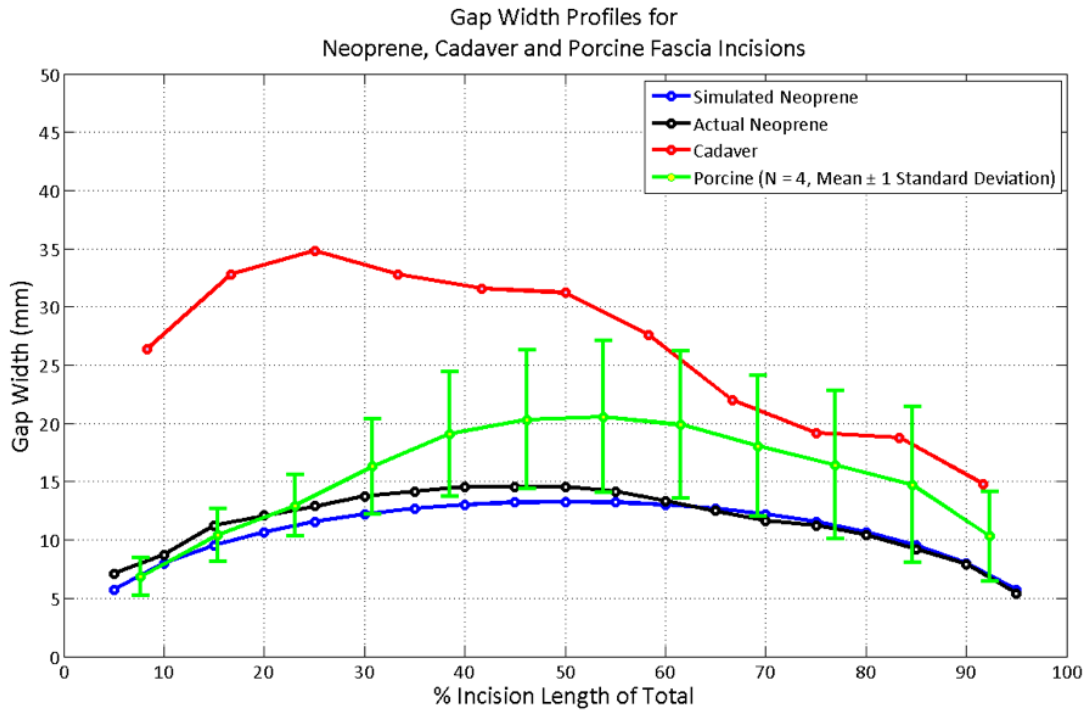
Figure 2.6: Illustration of the profile of the post-incision gap measured in a neoprene sheet, FE model of a neoprene sheet, and various abdominal fascia samples. Incision lengths along the midline varied between 18 and 22 cm.

2.3.2 Pull to Midline

The force needed to pull the actual neoprene back to midline at discrete locations spaced 1 cm apart along the incised gap edge was also in the same range as the forces predicted by individual pulls to midline of the computational FE model. The cadaver and porcine abdominal fascia required half to a third the amount of force needed for the neoprene. These results suggest that the stiffness of cadaveric and porcine abdominal fascia is lower than the thin neoprene sheet chosen as an abdominal fascia substitute. Figure 2.7 depicts the force needed to pull the incised tissue edge to midline one location at a time for the computational neoprene model, real neoprene sheet, as well as the cadaver and porcine abdomen preparations.

Force to Midline as a Function of Incision Length for
Neoprene, Cadaver and Porcine Fascia Incisions
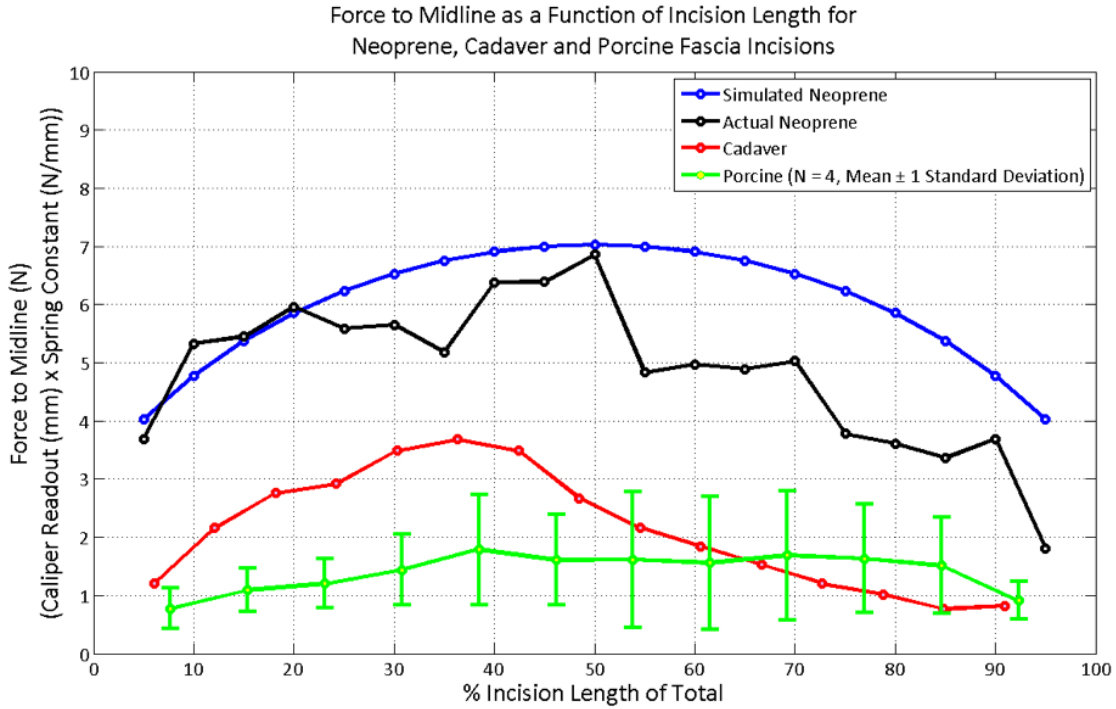
Figure 2.7: Force required to pull a neoprene sheet back to midline measured successively at regular intervals along the incision and as similarly measured on a virtual neoprene sheet and on various abdominal fascia tissues. Incision lengths varied between 18 and 22 cm

2.3.3 Displacement Fields

The comparison between the superimposed dotted grids of the stretched, incised and sutured real neoprene and the computational FE model illustrated that analogous treatment of the computational FE modelled neoprene to the physical neoprene placed on the simulator yields virtually identical amounts of stretch and deformation, not only around the vicinity of the crack, but throughout the material. Figures 2.8, 2.9 and 2.10 illustrate the superimposed actual and virtual neoprene materials, and the resulting local offset (in millimeters) between analogous points in the real (red) and virtual (blue) dotted arrays.

2.3.4 Suture Tension Required for Edge Apposition

The manipulation of suture bite (distance from location of tension applied to the crack edge) in the computational model revealed two important findings. First, the average tension required to pull the material edges back into apposition increased with an increase in suture bite. Second, analysis of the tension necessary to appose the material edges at discrete locations along the inci-
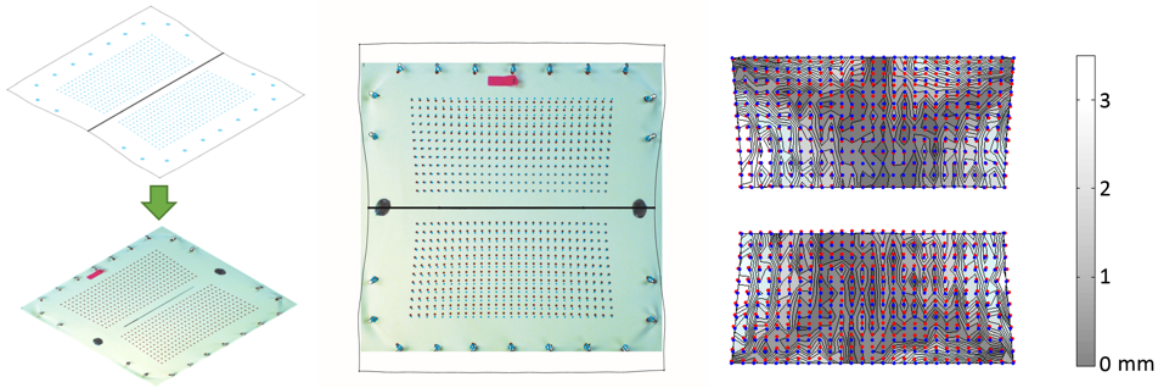
Figure 2.8: Comparison between virtual and neoprene materials as loaded onto the simulator platform, using a dotted array to denote deformations. The computational model is overlaid on an image of the stretched neoprene, such that virtual and physical anchoring locations are aligned (left). The stretched modeled and physical materials are shown in overlay (center). A contour plot is used to highlight the differences between corresponding grid point displacements in the computational and physical models (right).
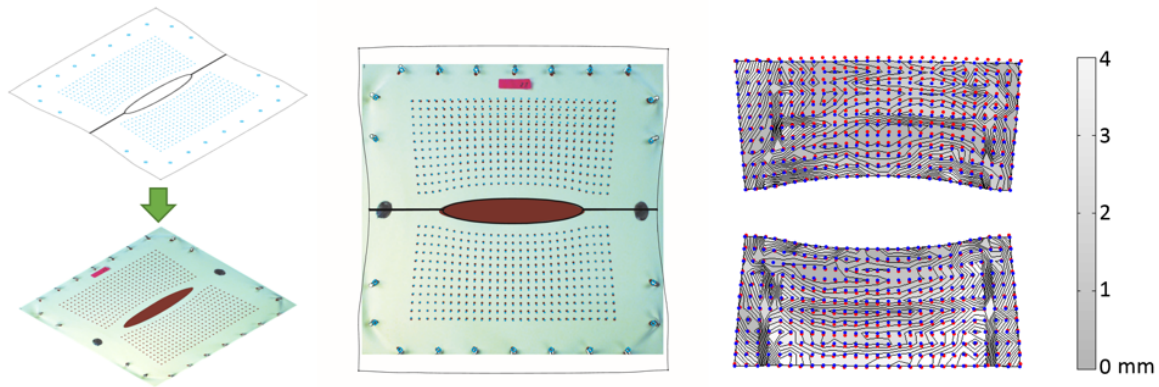
Figure 2.9: Comparison between virtual and neoprene materials as loaded onto the simulator platform, following a midline incision, using a dotted array to denote deformations. The computational model is overlaid on an image of the incised neoprene, such that virtual and physical anchoring locations are aligned (left). The incised modeled and physical materials are shown in overlay (center). A contour plot is used to highlight the differences between corresponding grid point displacements in the computational and physical models (right).

sion length revealed a non-uniform tension profile, with more force required to bring the middle of the incised edge back into apposition than the margins. Furthermore, this concave tension profile was most pronounced for small suture bites, and showed a tendency to flatten to uniformity as the suture bite size increased. The results of this computational analysis are shown in Figure 2.11.

19
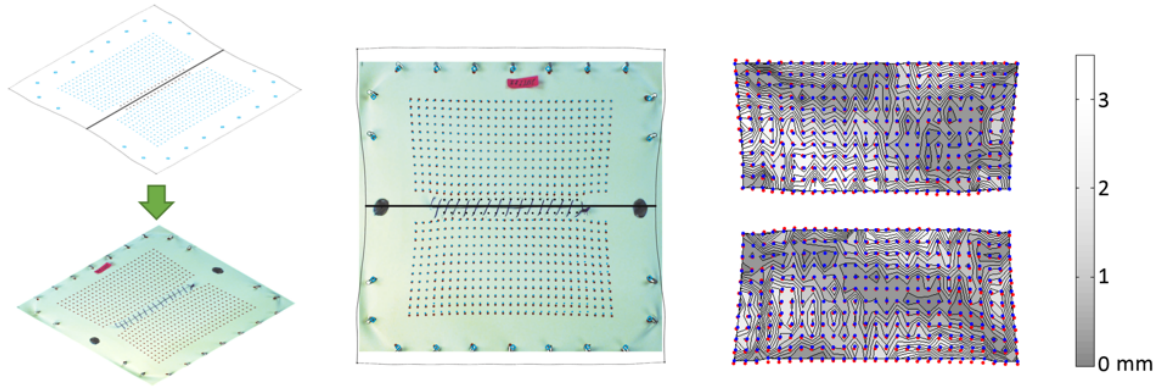
Figure 2.10: Comparison between virtual and neoprene materials as loaded onto the simulator platform, following a midline incision and continuous closure using a 1 cm bite to 1 cm travel ratio, using a dotted array to denote deformations. The computational model is overlaid on an image of the sutured neoprene, such that virtual and physical anchoring locations are aligned (left). The modeled and physical materials having undergone suturing are shown in overlay (center). A contour plot is used to highlight the differences between corresponding grid point displacements in the computational and physical models (right).
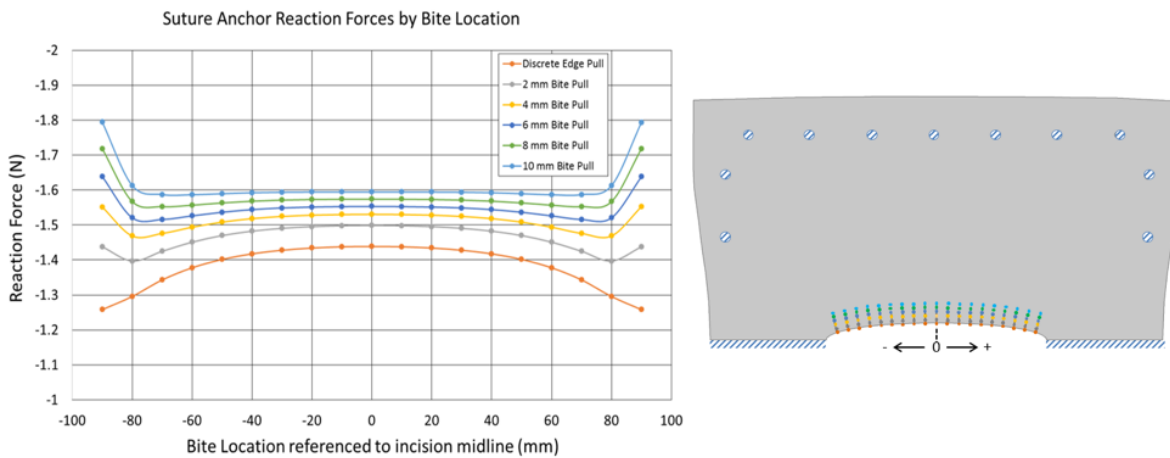
Figure 2.11: Suture reaction forces required for edge apposition computed at 19 uniformly spaced locations on a pre-stressed virtual neoprene half-plane model. Bite sizes (distance from the incision edge) of 0, 2, 4, 6, 8 and 10 mm are depicted. Bite locations are shown on the deformed virtual neoprene model on the right.

2.4   Discussion

Though stiffer than abdominal fascia, neoprene was found to best mimic the feel of puncturing the material with a needle and the tension applied to suture in order to bring the incised material edges back to midline using a continuous closure. Once incised, the elliptical gap resulting in the real neoprene material was smaller than the gaps recorded in the incised profiles of biological tissue. This is partially due to the higher stiffness of neoprene, and its fairly linearly isotropic material properties for deformations not exceeding 15% [49] unlike the material properties of abdominal fascia [48]. However, the larger incision gaps observed for cadaver and porcine abdominal fascia samples are also the result of released intra-abdominal viscera such as omentum and the small bowel, which would eviscerate above the incision edges when the abdomen was entered, and added to the observed separation of the abdominal incision. Artificial materials that have been specifically designed to mimic the loading, anisotropy and feel of abdominal fascia are available for purchase. However, their expense and special storage conditions when compared to neoprene make the latter ideal as a first pass material used to prototype a simulator for training abdominal closure technique. Future iterations of the physical simulator can also include simulated intra-abdominal viscera to further mimic the real condition of abdominal fascial closure.

The linearly elastic behavior of thin neoprene for the deformations to which it was subjected allowed us to compare the incision gap and resulting crack shape to well established previous research in the discipline of Fracture Mechanics. The incision gap profile and the major and minor diameter of the elliptical crack resulting from the biaxial stretch of the neoprene sheet is in agreement with theoretical work published on the subject of predicting crack propagation [43–45]. The displacement fields that can be extrapolated from the deformation of the dotted grid are likewise very informative, as they allow us to understand how local stresses affect the deformation of the material as it is stretched, incised, and then closed. One can thus assess whether a crack induced in a pre-stressed sheet of neoprene agrees with predicted local and/or global deformations caused by crack induction and propagation available in the literature. The dotted grid also allows for the quantification of local deformation in the neoprene material, under the different loading conditions, as depicted by the contour plots in Figures 2.8, 2.9 and 2.10.

The initial aim of employing a computational FE model was to assess the agreement between the deformation behavior of the virtual and actual neoprene sheets, using numerical methods and a solver based on energy methods. The simulation of the mechanical behavior of a thin neoprene sheet based on a computational model provides a couple of advantages. First, unlike biological tissues, thin neoprene is a linearly elastic material, making it easy to model for large applied loads and deformations up to 15% [49]. The ease of modelling and the wealth of contact mechanics research performed on linearly elastic materials allows us to develop an understanding of what is

going on as the neoprene is submitted to various mechanical loads. Second, the shape, loading, and deformation parameters of the neoprene sheet can be controlled much more precisely than live tissue samples. This allows the modeling of the virtual neoprene sheet dimensions precisely for simulation and comparative purposes. Third, the ease of mechanically loading neoprene under various conditions exceeds that of biological tissue, in which manipulation and the environment are critical parameters to be monitored. Briefly, one can repeatedly sample, deform and manipulate actual neoprene sheets in a precise fashion, while simultaneously applying the same manipulations to a virtual neoprene sheet in a computational FE model possessing the same material properties.

Contingent on the agreement between measured outcomes for the real and virtual neoprene sheet, the computational FE model can be used to extrapolate other results which may be difficult or time consuming to measure in reality, e.g. the forces needed to pull the incised neoprene edges back to midline as a function of suture bite and travel. The results of this analysis are shown in Figure 2.11.

Intuitively, pulling the material back to midline from locations farther away from the material edge requires higher forces overall. This can be explained by the fact that a shorter strip of material must be stretched as the anchoring location is increased away from midline. If it is assumed that the stiffness of the material is uniform, and discount the effect of neighboring strips on the material which are being stretched, then one can think of a strip of material as a finite collection of small springs linked to one another in series. As the location at which the stretch is applied is displaced further from the material midline, fewer springs in series are available to resist the material stretch. This could explain why the force required to pull the material to midline increases as the pull location increases relative to the midline.

Interestingly, the computational FE model predicts the force required to pull the material to midline to be highest at the center of the elliptical crack and decrease from there as the crack edges are approached. This is not intuitive because the material is initially displaced by the same amount longitudinally, so the amount of relaxation as the crack is induced should be uniform throughout. I performed a similar FE analysis on the virtual neoprene by imposing displacement constraints solely on the material edges parallel to the crack, and a similar force profile pattern emerged when simultaneous pulls back to midline at discrete but regularly spaced locations along the crack edge were performed.

Although more work is needed to assess whether the theory agrees with practice, anecdotal evidence provided by surgeons regarding the locations of abdominal herniation most often observed (at the middle of fascial closure) suggests that the forces needed to approximate the abdominal edges closed are indeed higher at the middle of the incision, and thus creates the location that is most at risk in the closure with any increased intra-abdominal pressure which places strain on the closure. This raises the question of whether an altered technique in closure at the middle of the

incision where tension appears to be highest is warranted and should be evaluated. The physical and computational models of abdominal fascial closure described here may provide a platform for evaluating alternate closure techniques which could lead to decreased hernia formation following laparotomy.

2.5   Future Work

The good agreement between the deformation of the thin neoprene sheet and its analogous computational FE model suggests that further work focusing on different closure treatments in the FE model should yield insight into how other closure types would affect the neoprene sheet. These include attempting midline incision closures with interrupted rather than continuous suture, the employment of friction in the suture tension model, as well as time dependent relaxation that may occur over time. The computational FE model could also be modified to behave anisotropically, and constitutive relationships could be modified to reflect nonlinear response under large deformations, as would biological fascia tissue, in order to assess whether the suture force closure profiles follow the pattern found in neoprene. The FE model could also be used to find the optimal suture tension and spacing for a wide variety of real and artificial abdominal fascia substitutes. This information could be presented as a function of the dotted grid deformation, and be used to better inform abdominal closure training protocols.

In parallel, I seek to use the image analysis algorithms performed on the dotted grid to better understand and quantify how experienced surgeons vary their suture spacing and tension on the neoprene loaded training platform. To that extent, my collaborators and I have started collecting neoprene closure data from our training simulator when closures were performed by surgeons and we have used the pre- and post-closure changes in the dotted grid to assess performance between subjects. We have incorporated the suture placement locations and dotted grid displacements into the computational FE model to extrapolate the amount of tension each suture loop contributes to the abdominal closure. Based on the dotted grid deformation, we seek to develop a numerical score and intuitive visual feedback that could be used to train closure consistency in both experienced surgeons and surgical residents. Our initial attempts at this goal are illustrated in Figures 2.12 and 2.13. To create a benchmark for optimal suture tension, 11 experienced surgeons were recruited to perform a simulated abdominal fascia closure on the neoprene impregnated surgical trainer. Pre- and post-suture images of these closures were used to assess the displacements of the dotted grid on the neoprene sheet, under the assumption that such displacement fields are indirect indicators of the amount of stress present in the material due to the suture tension required to close the incision. Post-suture images were also used to analyze the placement of each suture with respect to the incision line.

As a result, two types of visual presentations have been developed to provide feedback to leaners: The first, shown in Figure 2.12 displays the mean (yellow-dotted line) and standard deviation (green region) of the suture tension computed from the expert surgeon closures, as an approximate function of incision length. Nine additional traces in the figure depict the indirect tension measurements assessed for medical students recruited to test the surgical trainer. Displaying the optimal tension profile from the expert closures and the tension of an individual student in overlay is meant to inform the surgical trainee how their closure's tension matches the optimal tension throughout the closure. The second visual feedback shown in Figure 2.13 quantifies optimal suture placement in terms of size of top bite, bottom bite and travel between individual suture throws. On the left, expert regions for optimal bite and travel are shown as green bars, while the average bite and travel obtained from one trainee's closure are overlaid on top. This visual representation is complemented on the right by a schematic displaying how bite and travel parameters are measured in a closure. Future assessments of abdominal closures using medical students and surgical residents should inform the best visual means of providing suture tension and placement feedback. Assessments of performance and learning effects from a repeated measures human subject study would reflect whether such feedback is instructive and helpful.

This surgical training device represents a first-in-class product designed to inform a standardized metric in abdominal fascia closure. By providing medical students and novice surgeons with objectively taught and assessed feedback, I hope to contribute to a decrease in the incidence of the morbid complication of incisional hernia.
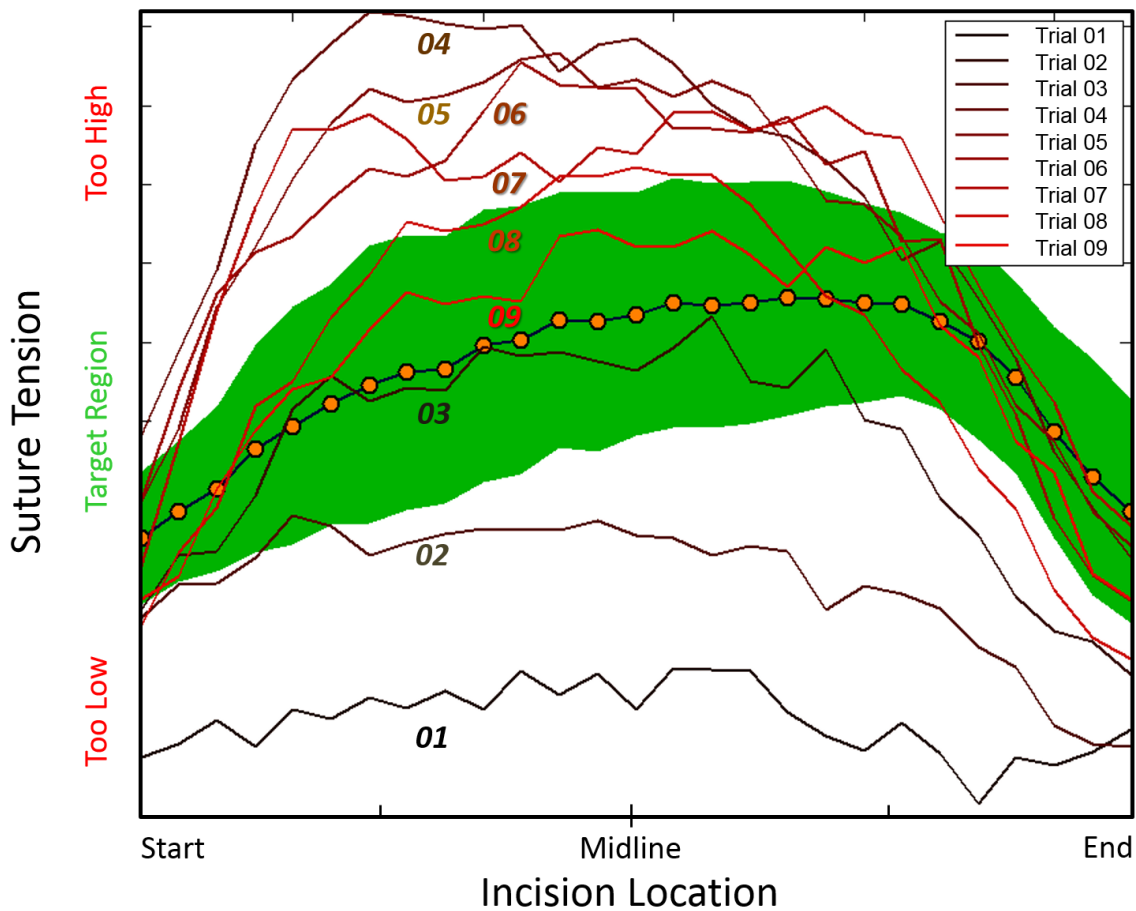
Figure 2.12: Mean (dotted yellow line) and standard deviation (green region) of the amount of tension employed by 11 expert surgeons to close an incision in a neoprene sheet, as a function of the location along the incision, using the surgical trainer. Suture tension is measured indirectly by assessment of the local displacement fields that appear in the dotted grid before and after the neoprene sheet is incised and closed. The numbered linear traces indicate the suture tensions obtained from various individual closures performed by medical students. Displaying the optimal expert-determined suture tension region and a trainee's performance in overlay as a function of location along the incision is one means of providing performance feedback to the user.
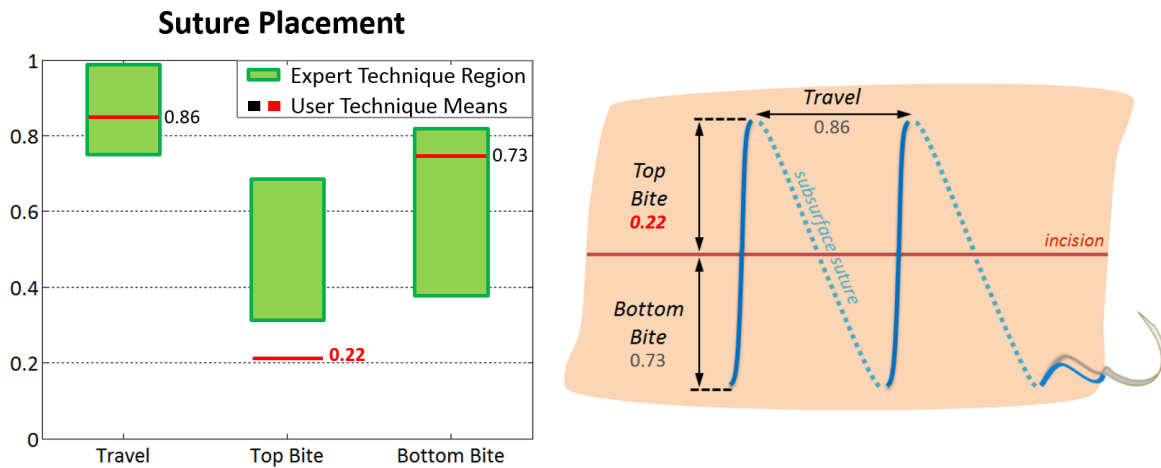
Figure 2.13: (Left) Standard deviation (green region) of top bite, bottom bite and travel obtained from the analysis of suture placement of 11 expert surgeons, displayed as a bar graph. A trainee's average suture bite size and travel is displayed as a line, with an adjacent numerical value. Image processing is used to assess the location and length of each suture throw with respect to the incision midline; these values enable the calculation of average top bite, bottom bite, and travel. (Right) Along with the performance feedback, a schematic is provided reminding the user how top bite, bottom bite, and travel are defined.

CHAPTER 3

Assessment of Neuromuscular Signals in-Vivo via a Novel Interface

3.1 Introduction

Up to one-third of upper limb amputees choose not to wear a prosthesis because currently available devices fail to provide sufficient restorative functions [50]. Advanced commercial devices such as the iLimb and Bebionic [51, 52] and research devices such as the DEKA and APL arms [53, 54] provide motorized joints that reproduce the motion, force production capabilities, and even offer instrumented fingertips that mimic the sensing capabilities of the human hand. However, a suitable control and sensory interface is not yet available to harness these functions.

The state of the art for determining the motor intent of an amputee is surface electromyography (sEMG), wherein the activations of one or more muscles in the residual limb or elsewhere on the body are transduced to produce signals for control of prosthetic motors. In the case of transradial amputations, residual muscles activated by the same neural circuits previously serving the lost limb are often available, thus providing a means to achieve 'intuitive' control. However, intuitive control is not available for wrist joint, metacarpal phalangeal joint or interphalangeal joint function in the case of proximal transradial, transhumeral or glenohumeral amputations, because none of the natively innervated muscles are present to provide these control signals. Use of surrogate muscles requires that the amputee learn to map the activation of surrogate neural circuits to the intended motions of the prosthetic hand. In practice, such mental operations preclude activating more than one joint at a time. Even with sEMG on the residual forearm, only one joint can typically be controlled at a time. Networks of sEMG sensors and sophisticated intent extraction algorithms have thus far demonstrated limited ability to reliably control multiple joints simultaneously [55].

The chief motivation for engaging the neural circuits that previously served the lost limb is to enable simultaneous smooth control of the multiple DOF built into an advanced prosthesis. The 'intuitiveness' of this interface control strategy has the potential to translate into smooth and fluid motions with less cognitive load. An additional advantage is that motor control and sensory

feedback is referenced to the phantom limb, enhancing the likelihood that the amputee will adopt the prosthesis into his or her body schema, i.e. to *embody* the device.

A number of approaches are under development to collect, parse, and transmit signals from the neural circuits originally serving the lost limb. These approaches include surface electrodes placed on skin atop reinnervated muscles, electrodes implanted in the central nervous tissue, electrodes placed in peripheral nervous tissue, and electrodes placed in muscle innervated by the peripheral nervous system, the feasibility of the latter having been demonstrated by Wells et al. in 2001 [56].

Brain Machine Interfaces show potential for controlling a high-DOF prosthetic device by recording the neural signals at their source. However, the use of cortical signals for control has only been demonstrated for periods on the order of months, [57, 58], whereas an interface is required that will last a lifetime. Signals can be acquired non-invasively using electroencephalography as well, though reliable control of high-DOF devices remains a challenge for this technology. An alternative means to engage the original neural circuits is to extract signals from the peripheral nervous system using pNG. However, signals extracted directly from peripheral nerves are characterized by amplitudes on the order of tens of microvolts and are prone to noise, interference from electromyographic signals from adjacent muscles, distortion from electrode displacement, and scarring of nerve tissue [25, 59]. While epimysial and surface EMG signals have sufficient amplitude relative to noise, they are only available from muscles in the residual limb that remain innervated. Thus EMG techniques are ineffective at providing hand function for a patient sustaining limb loss at or above the elbow. Even with transradial amputations, EMG signals from the intrinsic muscles of the hand are not available.

One of the most promising approaches for acquiring signals from the neural circuits originally serving the lost limb is TMR. One or more muscles no longer playing functional roles are identified and denervated, or, nerve endings are surgically coapted to nerve branches serving muscles exhibiting redundant function like the pectoralis. The nerves previously serving lost function are then surgically routed to these identified muscles, which they will reinnervate. Electrodes, often skin surface EMG electrodes, can then be used to record signals suitable for prosthesis control. The muscle serves as a signal transducer and biological amplifier for the signals transmitted in the peripheral nerves [28, 29]. By engaging muscles, TMR avoids direct contact between electrodes and delicate neural tissue. However, skin surface electrode displacement due to movement and sweat, a lack of alternate non-functional muscles and difficulty controlling the nerve fascicle migration (especially when fascicles are not well segregated by function) remains a limiting factor in the number of functionally independent DOFs that TMR can provide [60].

To engage the motor and sensory signals required for intuitive prosthetic control and to develop a reliable multi-DOF human-prosthetic interface, our research team proposes an approach that also uses muscle as a signal transducer, but one in which that muscle is both *regenerated and*

reinnervated. Rather than moving nerve to reinnervate muscle as in TMR, we propose to move muscle to nerve. Moving muscle involves an autologous graft, re-vascularization, regeneration, and reinnervation. First, a small free graft of autologous muscle tissue (about 1 cm in diameter and 2-3 cm long) is harvested from non-essential donor muscle. One or more nerve fascicles are dissected and surgically neurotized within the muscle graft. This muscle graft initially acquires nutrients from the local environment via imbibition, until a new vascular network is established. The attached nerve fascicles sprout nerve fibers that grow within the muscle tissue in search of new muscle fiber targets. Histological evaluations have demonstrated that reinnervation progresses in an orderly fashion through the muscle graft and healthy neuromuscular junctions are formed within rats in approximately 4 months [61]. Previous experiments have also shown that electrical stimulation of the peripheral nerve evokes compound muscle action potential (CMAP) as well as force transients [62]. These responses can be evoked without degradation in signal quality or amplitude for the 14 month lifetime of a rat [63].

While the use of free muscle grafts for transducing neural signals has been demonstrated to date only in rodents and primates, a unique development pathway exists in humans. Regenerated free muscle grafts have recently been used to treat persistent neuromas in patients who have sustained upper and lower limb amputations. Neuroma pain is commonly refractory to desensitization, biofeedback, medications, injections, and surgical nerve division. A graft of regenerated muscle can form a suitable target for nerve fascicles otherwise lacking a target, thus reducing the need for persistent axonal sprouting, elongation and subsequent neuroma recurrence. An electrode might be placed in or on that regenerated and reinnervated muscle to record a signal for prosthesis control. It is also possible to surgically dissect the nerve down to individual fascicles, each one of which would be used to reinnervate a separate grafted muscle [64]. Since the muscle grafts are quite small, many such grafts may be surgically prepared and placed in the human. By contrast, only two or three can be fit in the hind limb of a rat. Our research group envisions implanted electrodes with indwelling electronic circuitry for amplification, signal processing, and transdermal wireless transmission. The complete construct with regenerated, re-vascularized, and reinnervated muscle and implanted electrode bears the name RPNI.

Studies establishing RPNI function to date have only quantified the RPNI signals in response to stimulation of nerve in anesthetized rats. In this chapter, I contribute a demonstration involving awake, freely behaving rats, with the goal of establishing the utility of the RPNI for transducing volitional signals originating in the central nervous system central nervous system (CNS). I assess the viability of RPNIs as signal sources encoding voluntary hind limb locomotion during treadmill walking in rats. The main analytical metrics for RPNI characterization are signal amplitude and signal correlation with hind limb joint kinematics. I also assess signal artifacts by comparing RPNI outputs to analogous EMG outputs from Control rats whose surgical preparation only

involves electrode placement on intact hind limb musculature, and Denervated rats whose surgical preparation involves a neurectomy and electrode placement with no muscle graft. Signals are recorded from rats while ambulating on a treadmill. I expect similar signals from the RPNI and Control groups and quiescent signal from the Denervated group.

The results reported here complement previous investigations into the viability of grafted, regenerated muscle as a target for nerve reinnervation [61, 65], the use of electrodes and biocompatible polymers to harness the myoelectric signals generated by these constructs [66–68], potential signal interference generated by adjacent RPNIs [69], the use of partial muscle grafts for RPNI synthesis [70], and the long-term function of grafted muscle acting as a signal transducer [63]. The overarching goal of these collaborative studies has been to develop a high performance neural interface for communication between peripheral nerves and microprocessor controlled robotic prostheses, using muscle tissue as a signal amplifier and transducer. Together with the extensive data used to characterize RPNI function in anaesthetised rats to date, the features of RPNI signals acquired from awake, ambulating rats presented here demonstrate feasibility of the RPNI, and motivate further studies that would support translation of the surgical treatment and technology described herein to humans.

3.2 Methods

Six male 3-month-old F344 strain rats were used in this study. All animal care and use procedures were conducted in accordance with the National Research Council's *Guide for the Care and Use of Laboratory Animals* (1996) and were approved by the University of Michigan Animal Care and Use Committee.

3.2.1 Surgical Preparation

Three experimental groups of two rats each were devised: a Control group, Denervated group, and RPNI group. In the Control group the neuromuscular anatomy of the hind limbs remained intact. Rats in the Denervated group underwent right tibial neurectomy (soleus muscle denervation) and left peroneal neurectomy EDL muscle denervation). Rats in the RPNI group received a free right soleus muscle transfer to the right thigh, anterior to the biceps femoris, and neurotization with the proximal end of the transected tibial nerve, as well as a free left EDL muscle transfer to the left thigh, proximal to the biceps femoris, and neurotization with the proximal end of the transected peroneal nerve (Figure 3.1).

All rats received bipolar electrodes on the left EDL and right soleus muscles. The bipolar electrodes were formed by stripping approximately 10mm of insulation from each of two lengths of fine wire (Cooner Wire Corp., Model AS 631, Chatsworth, CA), fashioning loops of 3mm diameter from the bare wire and securing each loop with interrupted sutures to the epimysium of the EDL muscle 1.5 cm apart in the left hind limb, and to the epimysium of the soleus muscle 1 cm apart in the right hind limb. Next, the wired muscle grafts were wrapped in small intestinal submucosa (SIS) tissue repair biomaterial (Surgisis, Cook Biotech, West Lafayette, IN). The insulated electrode wires were routed below the skin to the upper back, where approximately 4 cm was looped and secured under suture-closed skin.

Each rat recuperated for 4 months to facilitate wound healing and reinnervation of the free muscle graft. On the day of an evaluation (within the fourth month after surgery), each rat's hind limbs were shaved; on the bare skin, non-toxic clay based paints were used to mark the positions of the hip, knee, and ankle joints, as well as the distal end of the paw. A short cutaneous incision on the upper dorsum was also performed to access the wire electrode ends and connect them to the EMG recording apparatus.

3.2.2 Recording EMG in Vivo

Rats were conditioned to walk on a rat treadmill (Columbus Instruments, Columbus OH) at constant pace between 8.5 and 9.0 m/min. Two synchronized 120 frames per second high speed
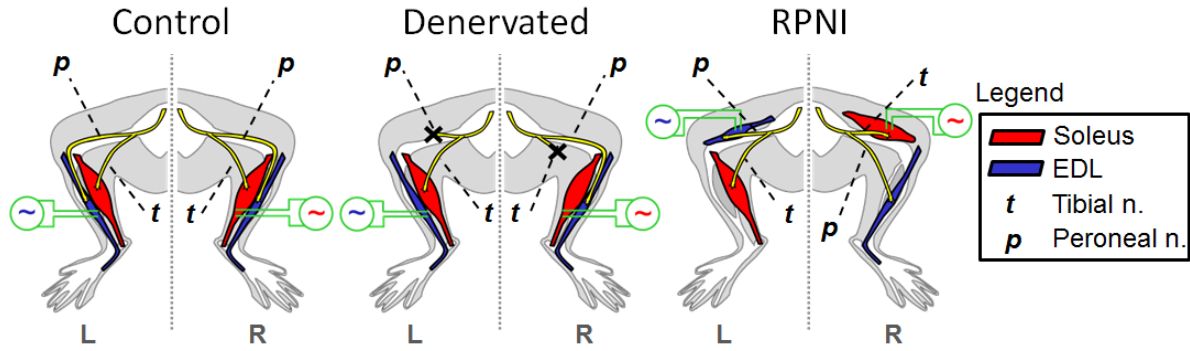
Figure 3.1: Schematic Diagram of the posterior view of the left and right hind limbs, indicating nerves (yellow, t=tibial, p=peroneal), muscles (red=soleus and blue=EDL), and electrode placement (green schematic) for the Control, Denervated, and RPNI study groups. In all rats, bipolar myoelectric signals originated from the surface of the EDL muscle on the left and soleus muscle on the right, with reference hook electrode in the left ear (not shown). The only surgical intervention for rats in the Control group involved electrode placement. Rats in the Denervated group received left EDL and right soleus neurectomies. Rats in the RPNI group underwent a free EDL muscle transfer with placement of the peroneal nerve for reinnervation on the left and a free soleus muscle transfer with placement of the tibial nerve for reinnervation on the right.

cameras (GoPro Hero2, San Mateo, CA) were positioned with their field of view perpendicular to the rat's walking direction and activated through a digital trigger (Figure 3.2). Myoelectric signals were amplified and bandpass filtered (1-500 Hz) with the use of a custom-built analog bipolar instrumentation amplifier. A nominal gain of 1000x was used and signal amplitudes were calibrated using a function generator and oscilloscope. The amplified and filtered signals were acquired at a 3 kHz sampling rate; during post-processing, the signals were digitally rectified and zero-phase low-pass filtered to 50 Hz. An LED positioned within the field of view of both cameras was toggled off and on through a button press, and recording of the LED control signal by the data acquisition system facilitated synchronization between the video and myoelectric recordings.

3.2.3 Acquiring Hind Limb Movement & EMG During Walking

A custom video and data processing program was written in MATLAB (Mathworks, Natick, MA) to facilitate synchronization of the video and myoelectric recordings and extraction of hind limb kinematics from the video. Within the video processing program, a computer vision algorithm was written in MATLAB to extract centroid locations for each of the hip, knee, ankle, and toe color markers appearing in each frame of the video recordings. These centroid locations were
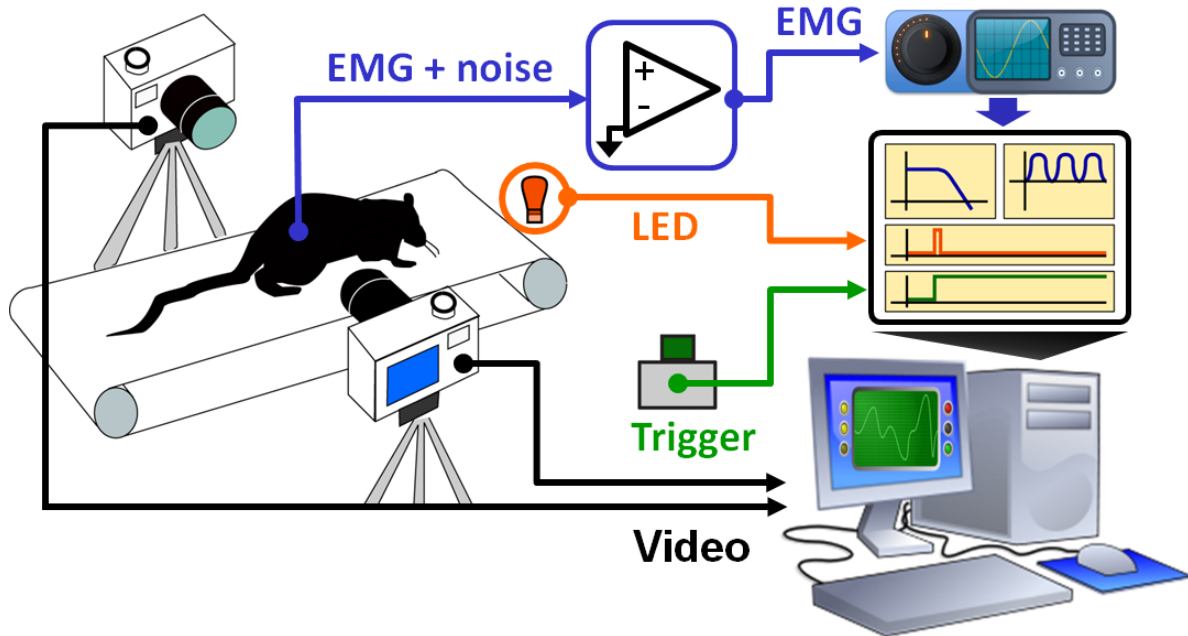
Figure 3.2: Depiction of the Data Acquisition Setup used to collect and analyze myoelecric and kinematic data. Myoelectric signals (blue) were amplified through an instrumentation amplifier, bandpass filtered (1-500)Hz, then digitally sampled at 3KHz. Offline, the data were rectified, and filtered again (0-50Hz). Myoelectric recordings were synchronized to high speed video recordings via the use of the LED and its control signal (orange). A triggering circuit and signal (green) were used to remotely start the video recordings bilaterally.

used in turn to identify hip, knee, ankle and toe joint angle trajectories bilaterally. Figure 3.3B contains pictorial definitions of the hip, knee, ankle, and toe angles. Left side and right side video recordings, the LED control signal, the extracted kinematic data, and the myoelectric recordings were visualized simultaneously onscreen to facilitate validation of the synchronization and extracted kinematics. Figure 3.3A presents screenshots, showing how the identified centroids and limb segments were displayed in overlay on the video recordings. The visualization program's user interface also supported the addition of gait event markers to the dataset. Thus gait events indicating foot landing and lift-off were added to each dataset, allowing the categorization of the gait data into periods of stance (landing to lift-off) and swing (lift-off to landing).

The extracted kinematic and EMG data was spliced into bouts, wherein each bout contained data for four or more complete steps. Walking was defined as a bout during which at least one hind limb was touching the treadmill belt continuously. Sequences in which the rat was standing still or hopping were removed. This spliced data was used to: 1) assess instantaneous EMG signal strength during walking cycles, 2) assess the cross-correlation between ankle joint kinematics and EMG
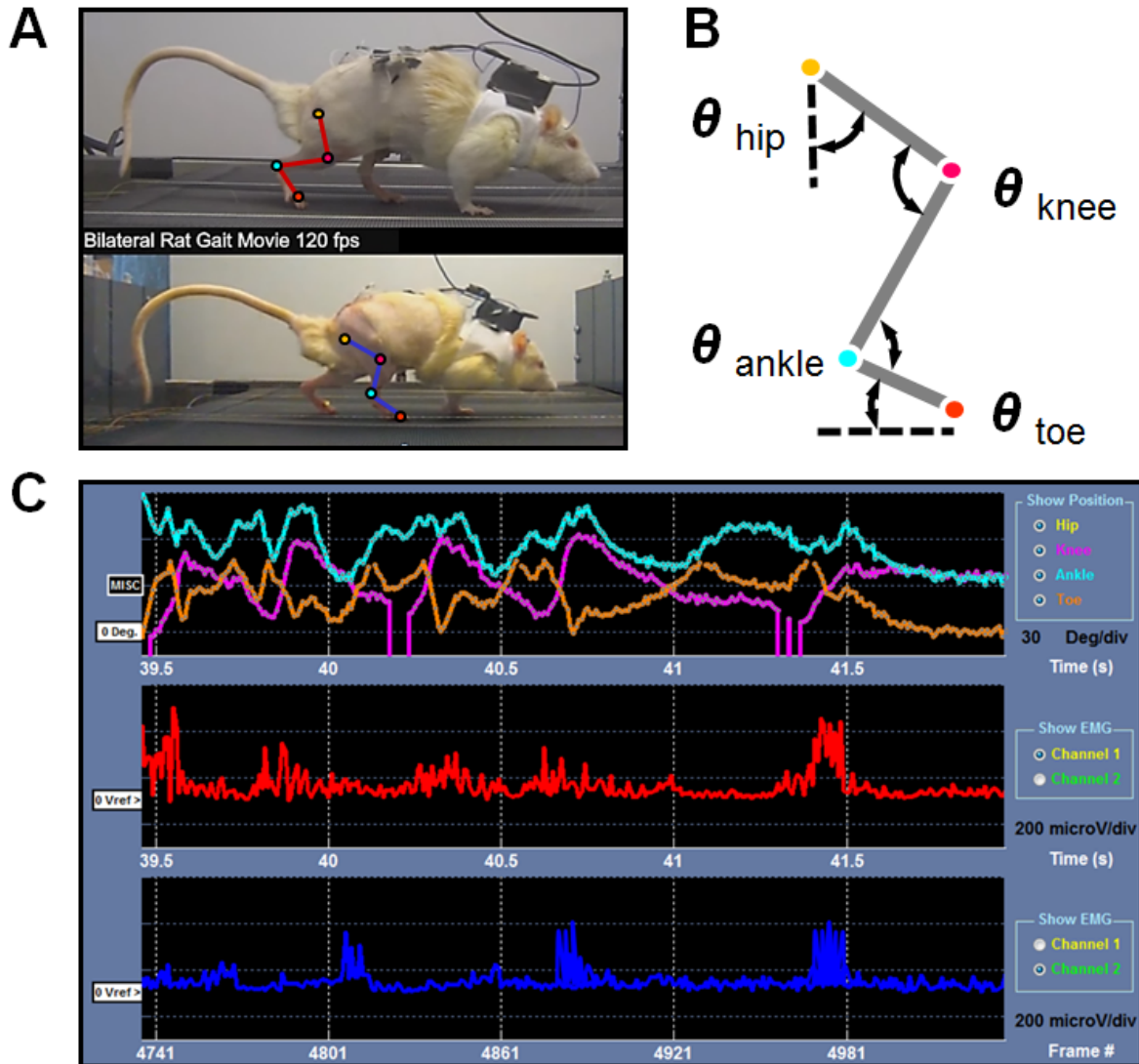
Figure 3.3: **A.** Illustration of the synchronized videos of the left and right leg of one rat during treadmill walking. A semi-automated method was used to detect the markers of the hind limb joints and create a stick figure model of the leg. Note that the video frames belonging to the rat's left hind limb were flipped vertically so that, for analysis purposes, walking appeared to occur in the same direction. **B.** A stick figure indicates joint angle references (positive as drawn) defined to describe hind leg kinematics. **C.** Synchronized traces of joint angles and bilateral myoelectric data (left leg, blue), (right leg, red) are shown.

data between groups, 3) quantify periodicity via power spectral density (PSD) in the frequency domain, 4) calculate the expected average EMG and hind limb joint kinematics during a single step, as well as 5) build a linear regression decoder, as discussed below.

3.2.4 Relating Observed Gait to EMG

To assess instantaneous myoelectric signal strength from all groups, the root mean square value (RMS) of the raw EMG voltage values collected during all walking trials was calculated. A linear mixed model with a random intercept per animal, and fixed effect for experimental level was employed to assess whether differences in recorded RPNI signals occur as a function of the surgical intervention. The model also employed a fixed term, the time at which the signal was measured in the study, in order to assess the sequence effect of the repeated measures obtained per rat (i.e. a linear trend with a random slope). Subsequently, cross correlation analyses between the rectified and filtered EMG and ankle joint kinematics obtained during walking trials were performed using PASW Statistics 22, (SPSS, IBM Inc., 2013, Armonk, NY). Then the PSD of the EMG signal and of the ankle angle derived from the kinematic analysis for all continuous walking bouts were computed using the $periodogram$ function in MATLAB on the raw signals (without normalizing time).

Finally, for the purpose of comparing kinematic and EMG data between groups for an average step, hind paw gait events were used to segment the kinematic and EMG recordings into stance and swing phases of gait for each leg. Stance was defined between the hind paw making contact with the treadmill (landing) and subsequent liftoff. Swing was defined between liftoff and the next landing event. Each gait cycle (including kinematic and myoelectric recordings) was time-course normalized such that the beginning of stance corresponded to 0% and end of swing corresponded to 100% of gait for either hind limb. Within each experimental group, normalized kinematic and myoelectric recordings were aligned using the landing gait events before being used to compute a mean and standard deviation representative of a single step for all joint angles and EMG data.

3.2.5 Decoding Gait Patterns from EMG

To further assess the relationship of the myoelectric signals to the gait kinematics, a linear decoder [71,72] was constructed for each rat leg. The decoder is based on a general linear model that attempts to reconstruct the hind limb trajectories using the simultaneously occurring EMG signal along with delayed versions of that same EMG signal. Half of the dataset for one rat comprising recorded myoelectric signals and extracted kinematic variables was used to construct a regression matrix $\mathbf{A}$. The second half of each dataset was then used to assess the predictive power of the model contained in $\mathbf{A}$. Kinematic variables were modeled as a function of EMG variability, using a linear Wiener filter, determined by a multidimensional linear regression, as per Equation (3.1).

In detail, the myoelectric signal was used to construct a $n \times 20$ matrix $\mathbf{X}$, where n is the number of data points and each of the 20 columns contains the processed myoelectric signal with an increasing time lag. Thus the first column has no lag while the 20th has 20/120 sec. of lag. (The

myoelectric signal was resampled at 120 Hz to match the motion capture camera framerate.) The kinematic variables for the hip, knee, ankle and toe were used to construct a $n \times 4$ matrix $\mathbf{Y}$. Then the general linear model:

$$\mathbf{Y} = \mathbf{X}\mathbf{A}, \tag{3.1}$$

was solved for the regressor matrix $\mathbf{A}$ using the pseudoinverse:

$$\mathbf{A} = (\mathbf{X}^T\mathbf{X})^{-1}\mathbf{X}^T\mathbf{Y} \tag{3.2}$$

The decoder was supplied with a 10 step training dataset and 10 step validation dataset from each rat and was trained separately for each rat (and each leg) used in the study. To assess the decoder's performance on each leg, the coefficient of determination (R^2) metric was used,

$$R_i^2 = 1 - \frac{\sum_{t=0}^{N} \left(\widehat{f_i(t)} - f_i(t) \right)^2}{\sum_{t=0}^{N} \left(f_i(t) - \overline{f_i(t)} \right)^2} \tag{3.3}$$

where $f_i(t)$ is the ankle joint angle from the ith leg, $\widehat{f_i(t)}$ is the corresponding estimate from the decoder, $\overline{f_i(t)}$ is the temporal average of $f_i(t)$, N_i is the number of data samples and R_i^2 is the coefficient of determination from the left or right leg.

3.3 Results

Raw EMG signals were more active with higher amplitudes during walking sequences than during periods of standing still in both Control and RPNI rats. Raw EMG signals in the Denervated rats showed very little activity regardless of whether the rat was walking or standing still. Figure 3.4 shows representative raw EMG traces obtained during a treadmill walking trial for a rat from each group. The traces are labeled according to whether the rats were walking or standing still. In particular, the signals recorded from both the left and right RPNIs during walking featured large excursions with amplitudes ranging between 0.75 to 1.0 mV_{PP}; during standing, the signal never exceeded 0.1 mV_{PP}. By contrast, the Denervated group demonstrated a very small amount of EMG activity throughout all treadmill locomotion trials, with a maximum of 0.2 mV_{PP}.
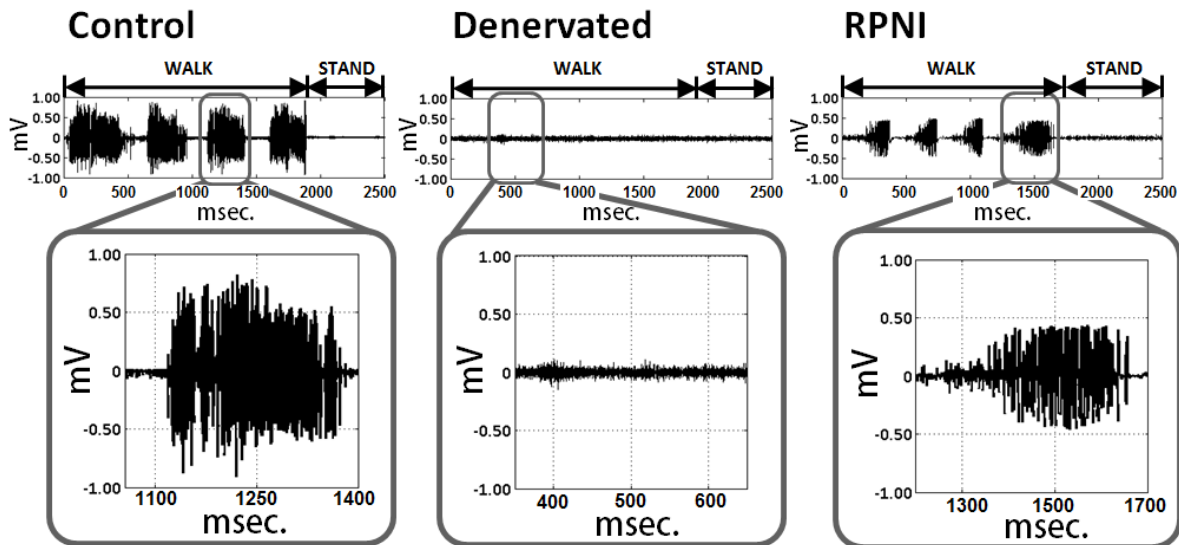
Figure 3.4: Raw signal depicting 4 strides followed by standing, obtained from the right leg of a Control, Denervated and RPNI rat. The signal corresponding to one stride from each group is enlarged for comparative purposes.

Walking EMG signal strength for each experimental group was quantified using the RMS of the signals. Linear Mixed Model predictions for the expected signal RMS per stride of Control, Denervated, and RPNI Rats, as well as the effect of Time at Evaluation on RMS are provided in Table 3.1. Figure 3.5 highlights the RMS values obtained for the left (blue bars) and right (red bars) legs at the time of evaluation post surgery, as well as the number of strides collected during each evaluation. It is immediately apparent that the Denervated group has low EMG signals, and that signal amplitudes do not vary appreciably over time for any experimental condition. Also, the RPNI signals were substantially greater than the Denervated group, but still somewhat lower than

Control.
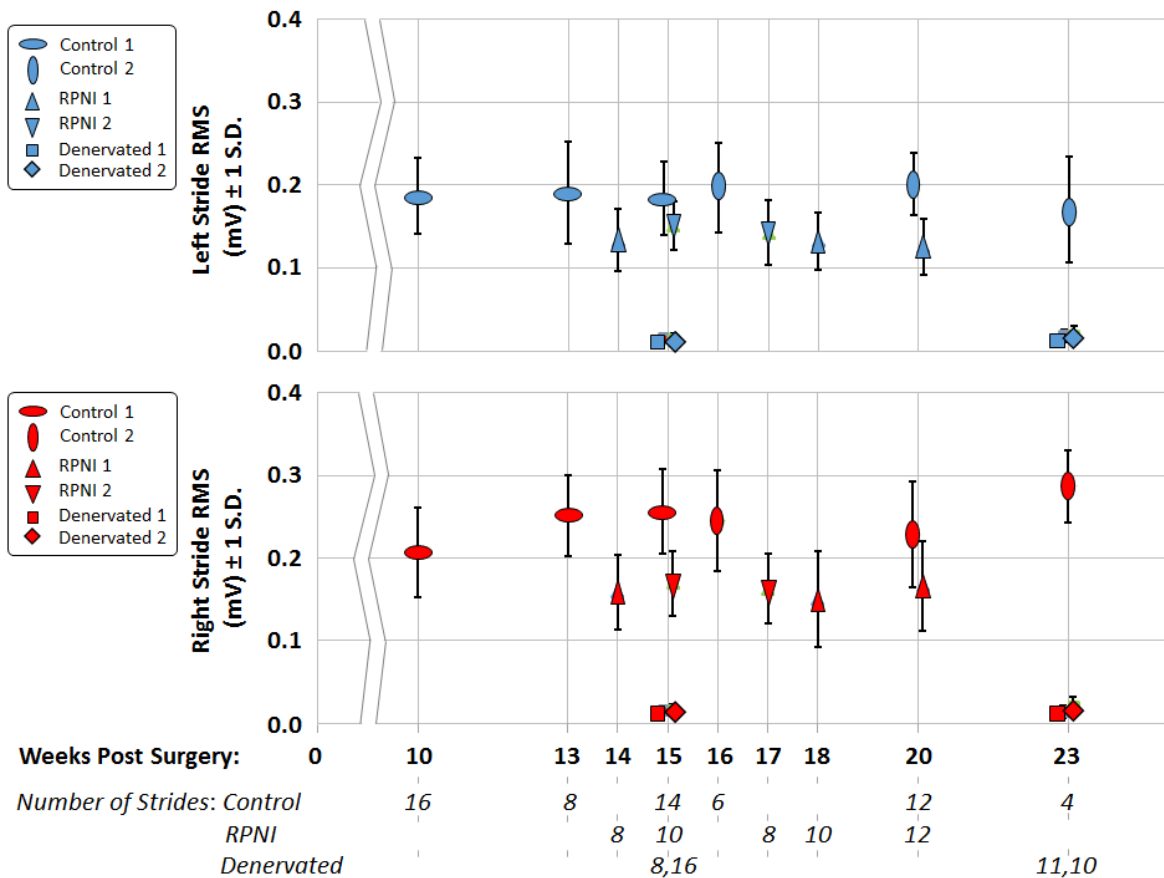
Figure 3.5: Root Mean Square $\pm$ one standard deviation of the EMG signals of EDL muscle reinnervated by the peroneal nerve (blue) and Soleus muscle reinnervated by the tibial nerve (red) obtained from bilateral gaits of Control, Denervated, and RPNI rat cohorts over a 13 week evaluation period. The data is sorted by week of evaluation post surgery, and number of bilateral strides collected for each observation.

Joint angle trajectories extracted from the video recordings during multiple strides (60 from the 2 Control rats, 45 from the 2 Denervated rats, and 48 from the 2 RPNI rats) and normalized in time to align foot landing events indicated a significantly altered gait in the Denervated and RPNI groups. The time-normalized records were then used to compute an average joint trajectory and standard deviation as shown in Figure 3.6. Joint angle trajectories for the Control group appear to be normal when compared to published data (compare the first column of Figure 3.6 to Figure 8 in ref. [73]).

As expected from the neurectomy performed in rats in the Denervated and RPNI groups, the right ankle exhibited an inability to plantarflex while the left ankle exhibited an inability to dorsi-

38

Table 3.1: Linear Mixed Model estimates and standard errors for the expected signal RMS (mV) accounting for the effects of the experimental group and time of observation (weeks post surgery). A $*$ corresponds to a significance level $p < 0.001$. The influence of the experimental group on predicted RMS signal amplitude is significant, while time of observation is not.

	Left Leg		Right Leg	
	Est. $\pm$ Std. Error	F(1, 149), Sig.	Est. $\pm$ Std. Error	F(1, 149), Sig.
Control	0.174 ± 0.007	570, $*$	0.218 ± 0.009	574, $*$
Denervated	0.019 ± 0.006	741, $*$	0.016 ± 0.007	738, $*$
RPNI	0.121 ± 0.007	264, $*$	0.145 ± 0.009	239, $*$
Time	-0.0001 ± 0.0003	$0.258, p = 0.61$	-0.0006 ± 0.0004	$0.253, p = 0.63$

flex. These observations can be made by comparing across the second and third columns in Figure 3.6. Figure 3.7 shows the same kinematic data in a marching frame stick figure for the left (blue) and right (red) hind limbs. As in Figure 3.6, time has been normalized to one stride and the right and left gait cycles have been time shifted to show liftoff at 0%. Thus, the similarity in gait between the Denervated and RPNI groups is also apparent when comparing the stick figures in the second and third columns of Figure 3.7. Also note that the liftoff markers for the left and right legs are aligned for the Control group but not for the Denervated or RPNI groups. Thus average stance time and swing time per stride were similar for both legs in the Control group but differed on the left and right legs in the RPNI and Denervated groups.

The EMG signal patterns, on the other hand, were different for all three groups. In particular, the EMG signal was essentially silent in the Denervated group. Directly below each of the stick figure plots in Figure 3.7, the time course averaged EMG signal from the EDL muscle on the left leg is shown in blue and from the soleus muscle on the right leg in red. Shaded regions behind the average trace indicate one standard deviation. The EMG patterns in Control rats are expected to differ between the right and left hind limbs, as they are derived from different muscles. Likewise, the EMG patterns in the two hind limbs from each of the RPNI rats are expected to differ because they are derived from muscles innervated with different nerves. Note that the EMG patterns from the RPNI rats differed significantly from those of the Control rats, just as the kinematics differed. In particular, the RPNI group EMG signals showed an altered activity profile during stance and minimal activation during swing.

Though different, the activation patterns of the EMG signals were strongly correlated with the
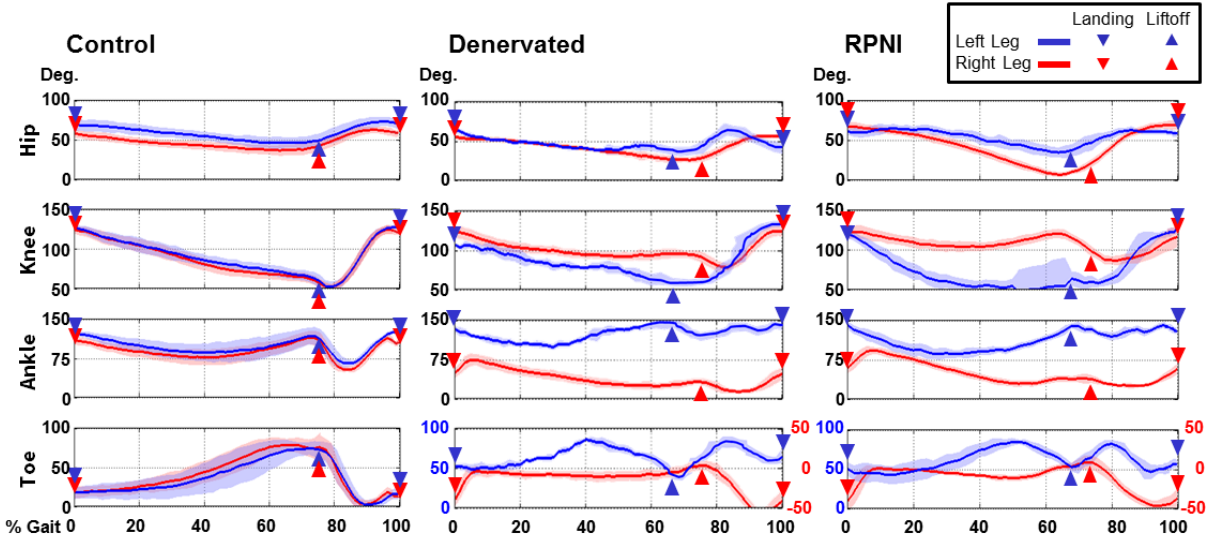
Figure 3.6: Time course average and standard deviation of joint kinematics, normalized with respect to gait cycle, and separated into stance and swing phase of EDL muscle reinnervated by the peroneal nerve (blue) and Soleus muscle reinnervated by the tibial nerve (red) from bilateral gaits of Control (2,60), Denervated (2,45) and RPNI (2,48) rat cohorts.

joint angles obtained from the Control and RPNI groups. Correlation between the acquired non-normalized EMG signal and the observed ankle joint kinematics was confirmed using the Pearson product-moment correlation coefficient; these values are provided in Table 3.2. The Denervated group demonstrated low amplitude random EMG activity, unrelated to gait.

The matching periodicity of ankle joint and EMG signals obtained from the Control and RPNI groups was assessed by computing the PSD for all walking bouts. This computation, performed on non-time course normalized data, yielded a power spectrum with signal peaks occurring at near 2Hz for both ankle joint and EMG in the Control and RPNI groups. This signal peak corresponds to 500 msec., or the average stride time observed in both groups. To assess that shifts in ankle angle and EMG periodicity are similar and could be observed during instances when rats walked slightly slower or faster than average, the PSD for ankle and EMG data from each bout was calculated bilaterally. Spectra were plotted in top-down view using color to visually scale signal intensity. Figures 3.8 and 3.9 depict the PSD plots of ankle joint and EMG obtained from ten bilateral walking bouts of RPNI rats.

To further explore the relationship between the EMG signal and ankle kinematics during walking, I constructed a linear decoder for each of the three groups. The kinematic outputs of the linear decoder for a four step EMG input of a Control, Denervated, and RPNI rat are shown in Figure 3.10. Linear decoder performance indicates a strong correlation between the joint position and

40
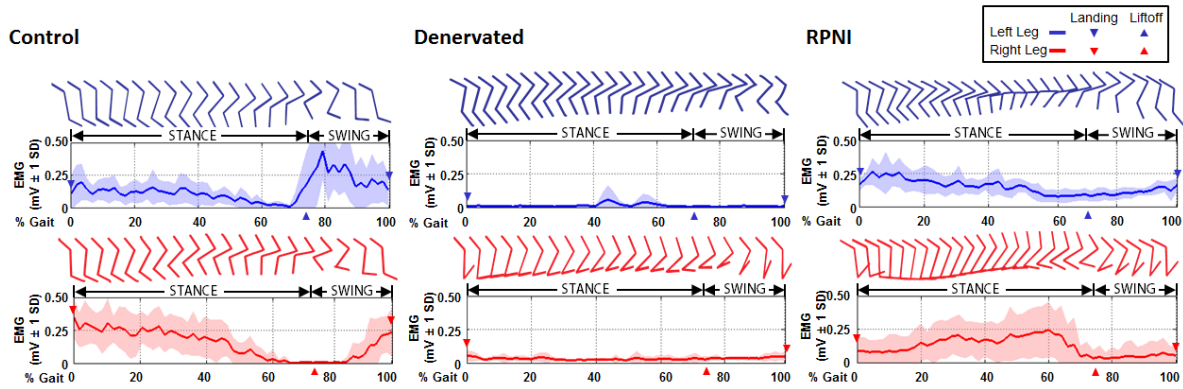
Figure 3.7: Time course average joint kinematics modelled as a three segment limb and mean ± standard deviation myoelectric activity, normalized with respect to gait cycle, and separated into stance and swing phase of EDL muscle reinnervated by the peroneal nerve (blue) and Soleus muscle reinnervated by the tibial nerve (red) from bilateral gaits of Control (2,60), Denervated (2,45) and RPNI (2,48) rat cohorts. As expected, the zero phase shifted joint kinematics of the left and right leg in Controls is similar, while the EMGs originating from antagonist pair of muscles are different. Note that for the Denervated and RPNI rats, the surgical intervention eliminated hind limb dorsiflexion on the left and plantar flexion on the right.

EMG signal for the Control and RPNI rats. By contrast, the low, random EMG signals acquired from Denervated rats shows very little resemblance to hind limb motion. Decoder performance for all rats used in this study are summarized in Table 3.3.

41

Table 3.2: Kinematic data and myoelectric signal correlation between observed bilateral ankle joint position and recorded EMG activity during treadmill walking.

		Control		Denervated		RPNI	
		C1	C2	D1	D2	R1	R2
Rat ID							
Strides		38	22	26	19	26	22
Pearson's r	Left	0.86	0.89	0.21	0.25	0.74	0.80
	Right	0.85	0.87	0.25	0.31	0.78	0.79

Table 3.3: Estimation Accuracies $R^2(\%)$ Results of decoder performance for each rat used in the study.

		Control		Denervated		RPNI	
		C1	C2	D1	D2	R1	R2
Rat ID							
$R^2(\%)$	Left	88.1	87.0	14.9	10.7	78.8	83.5
	Right	92.8	94.2	16.4	12.2	83.1	80.3
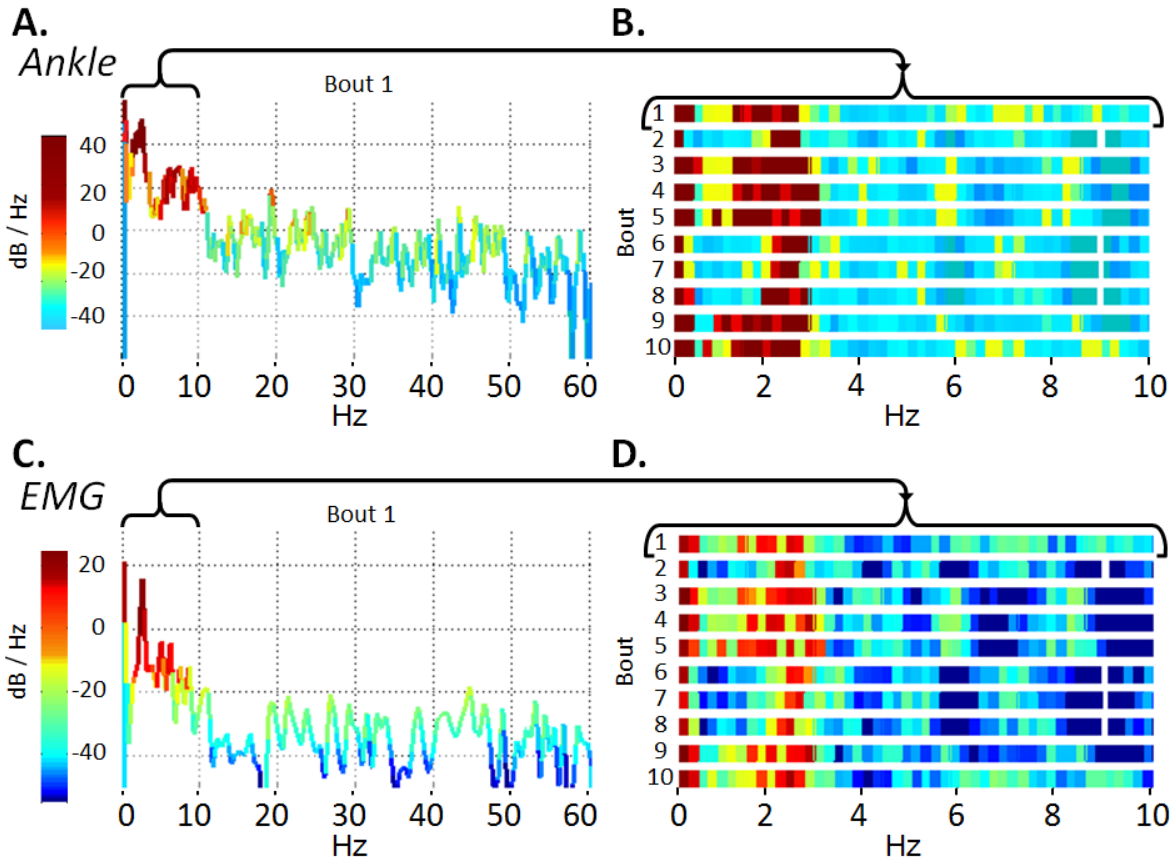
Figure 3.8: Power Spectral Density Plots for ankle kinematics (top) and myoelectric (bottom) data obtained from the left leg. **(A.)** Plot of ankle kinematics from first Bout (4 continuous strides) of an RPNI rat during treadmill walking. **(B.)** Top view of the Power Spectral Density plots of 10 Bouts containing kinematic data obtained from both RPNI rats, focusing on the 0-10 Hz frequency range. **(C.)** Plot of EMG signal obtained from first Bout (5 continuous strides) of an RPNI rat during treadmill walking. **(D.)** Top view of the plots of 10 Bouts containing EMG data obtained from both RPNI rats, focusing on the 0-10 Hz frequency range. Contour colors scale to signal power amplitude for adjacent plots.

3.4 Discussion

The primary aim in this study was to determine the strength, viability, and the extent to which RPNI signals are correlated with motions produced by awake rats walking on a treadmill. By assessing the correlation between the RPNI signal and observed movement, I aimed to gauge whether the RPNI is transducing the locomotor commands relayed from the CNS to the hind limb via the associated peripheral nerve. Although the surgical intervention produced significant
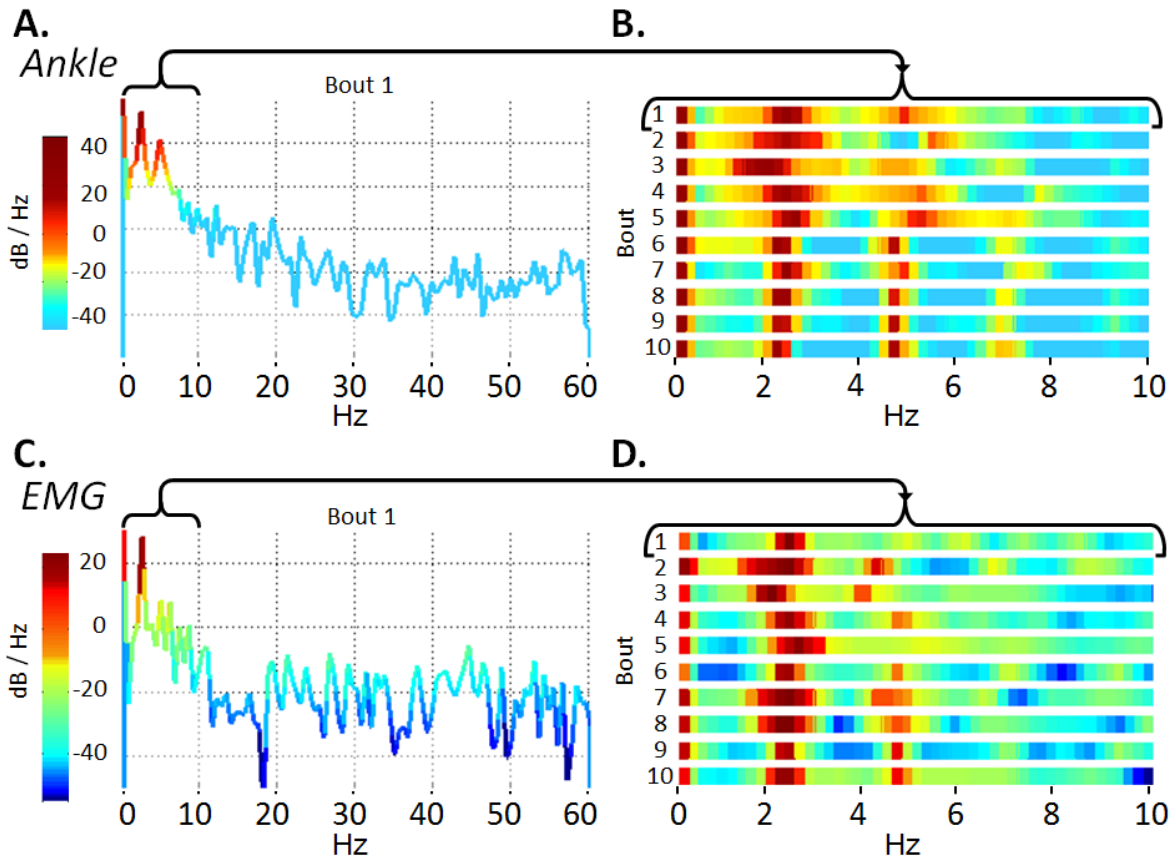
Figure 3.9: Power Spectral Density Plots for ankle kinematics (top) and myoelectric (bottom) data obtained from the right leg. **(A.)** Plot of right ankle kinematics from first Bout (5 continuous strides) of an RPNI rat during treadmill walking. **(B.)** Top view of the plots of 10 Bouts containing kinematic data obtained from both RPNI rats, focusing on the 0-10 Hz frequency range. **(C.)** Plot of EMG signal obtained from first Bout (5 continuous strides) of an RPNI rat during treadmill walking. **(D.)** Top view of the plots of 10 Bouts containing EMG data obtained from both RPNI rats, focusing on the 0-10 Hz frequency range. Contour colors scale to signal power amplitude for adjacent plots.

alterations to the gait of the Denervated and RPNI rats, a strong correlation was observed between the acquired signals and hind limb joint kinematics in the RPNI rats, similar in amplitude and periodicity to signals from Control rats. These findings support the claim that the muscle in an RPNI, once regenerated and reinnervated, can function as a biological amplifier for the signals transmitted through a peripheral nerve.

44
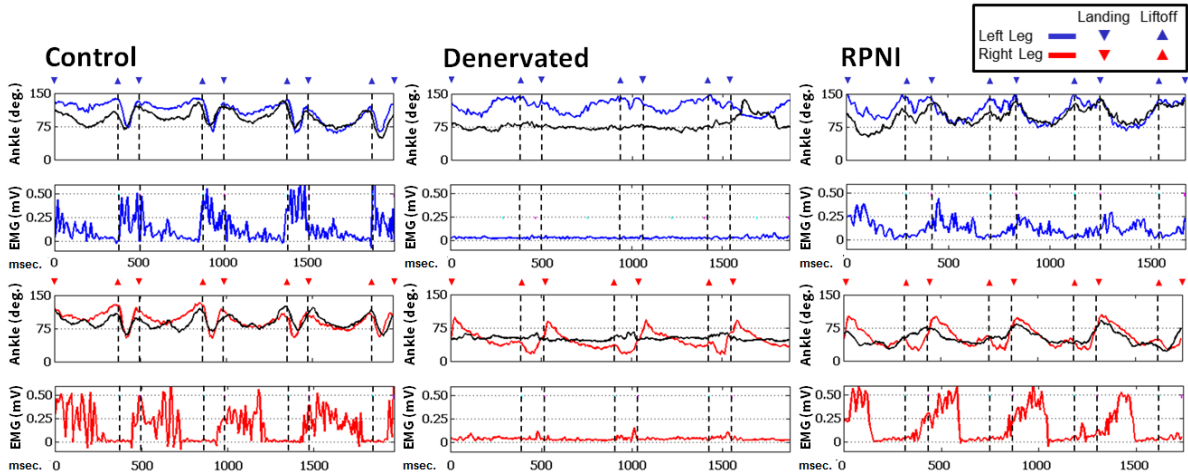
Figure 3.10: Actual ankle kinematic and myoelectric data used to train a decoder from four left leg (shown in blue) and right leg (shown in red) gaits of a Control, Denervated and RPNI rat. Black traces correspond to the decoder-generated kinematic data for each leg of each rat.

3.4.1 RPNI Signals Exhibit Large Amplitudes

One of the most noteworthy features of the RPNI signal is its large amplitude relative to direct recordings from the peripheral nerve. In its raw form, the maximum amplitude of the RPNI signal was on the order of 1.0 mV$_{\text{PP}}$ (Figure 3.4, third column). By comparison, peak amplitudes published for intraneural signals recorded during motor function in awake rats using intrafascicular wire electrodes do not exceed 0.01 mV$_{\text{PP}}$ in the sciatic nerve [59]. Regenerative intra-axonal microchannel electrodes, which interface directly with individual axons, can deliver signal amplitudes up to 0.2 mV [22, 24], but require a well-shielded environment to prevent signal corruption by active adjacent muscle, as well as minimal neural injury for adequate longterm function [25]. The factor of 10-100 by which the RPNI signal is larger reflects the advantage that signals acquired using epimysial electrodes enjoy over signals acquired using intraneural electrodes.

The RPNI signal is similar in amplitude to signals recorded from ambulating rats using epimysial electrodes by our group and others [73]. The similarity to epimysial EMG recordings is to be expected since RPNI signals are acquired using implanted electrodes placed on muscle. RPNI signal amplitude, though significantly higher than recordings obtained using intraneural electrodes, is 20-25% smaller than EMG signals acquired from the same epimysial electrodes from rats in the Control group. This 20-25% degradation relative to Controls has also been observed in studies on the RPNI involving anaesthetized rats [61]. The smaller amplitude likely stems from the tendency of the regenerated and reinnervated muscle grafts in the RPNI to contain a larger component of non-myocytic tissue, which could impede signal flow to an epimysial electrode, as observed in

the histological studies reported in [61]. The reason for this may be partial muscle atrophy upon re-grafting, until tissue revascularization and nutrient imbibition takes place on a large enough scale.

3.4.2 RPNI Signals Not Corrupted by Cross-Talk

To characterize the signal-to-noise ratio in the RPNI signal, it was assumed that the underlying neural signal in both Control and RPNI rats is completely quiet during periods of hind limb inactivity or standing. Under this assumption, the noise amplitude is on the order of 50-100 μV_{PP} (raw signals from Control and RPNI groups during standing, see Figure 3.4). If one interprets the maximum amplitude of 0.75 $\mathrm{mV_{PP}}$ for Control and 0.45 $\mathrm{mV_{PP}}$ for RPNI as an information-carrying signal, a signal-to-noise ratio of 17.5 dB and 13.0 dB s obtained for Control and RPNI, respectively.

Signals from the Denervated group were consistently low (see Figures 3.4 and 3.5). Although rats in the Denervated group had epimysial electrodes placed in non-innervated muscle, those electrodes could have transduced motion artifact or activity from antagonist muscles nearby that were still innervated and active. The consistently low signal amplitudes obtained from the Denervated group are reassuring, as it indicates that signals from target muscles would not be masked by motion artifact or crosstalk from neighboring muscles.

3.4.3 Signals Active During Walking, Quiet During Standing

Periods during which EMG signals from the Control and RPNI groups were active correspond to periods of treadmill walking, while periods of low signal activity correspond to periods of standing. This correspondence supports the claim that these EMG signals were centrally generated. To further assess the correspondence between signal and observed hind limb kinematics, I segmented the recordings and computed RMS amplitudes during periods of walking and standing. Signal amplitudes were significantly higher during walking than standing (see Figure 3.4).

3.4.4 Signals Periodic with Gait

Though different, the activation patterns of the EMG signals and joint angles obtained from the Control and RPNI groups were periodic with gait. A correspondence among patterns in the RPNI signal and the gait can be recognized in the mean RPNI signals and mean kinematic trajectories, obtained after time course averaging (Figure 3.6). The consistently low amplitude myoelectric signal from the Denervated group is immediately apparent in Figure 3.7. The RPNI signals in contrast have peak amplitudes similar to the recordings from the Control group. Moreover, both the

Control and RPNI group myoelectric signals are patterned with the gait, which is further evidence for the existence of periodicity in the signal. In contrast, the Denervated group demonstrated low amplitude random EMG activity, unrelated to gait.

As a result of transecting nerves in the preparation of the RPNIs, certain functions in the right and other functions in the left hind limb were extinguished. Consequently, the gait of the RPNI group rats was significantly different than the gait in the Control group (Figure 3.6, first and third columns). The same nerves were transected in the Denervated group as the nerves transected and used to reinnervate the RPNIs in the RPNI group. As expected, the gait of the rats in the Denervated group was similar to the gait of the rats in the RPNI group (Figure 3.6, second and third columns). Specifically, the left hind limb of rats in the RPNI and Denervated groups underwent a complete transection of the peroneal nerve, compromising dorsiflexion and the function of all muscles in the anterior compartment. Thus one observes less dorsiflexion in the left hind limb, which is particularly noticeable during swing (see blue stick figures in Figure 3.7). The right hind limb of the rats in the RPNI and Denervated groups underwent a transection of the tibial nerve, producing an expected loss of plantarflexion, which is particularly noticeable during stance (see red stick figures in Figure 3.7).

The altered gait may explain the difference in EMG activity recorded from RPNI rats relative to Control rats, especially during swing. The normal phase antagonism between EMG signals from the left and right hind limbs is essentially lost in the RPNI rats, just as phase relationships in the kinematics of the left and right hind limbs are lost in the RPNI and Denervated rats. Presumably, the descending neural control signals are also significantly altered to compensate for the surgically altered mechanics of the hind limbs, a finding not unlike the abnormal EMG locomotion patterns observed by Gramsbergen et al. following sciatic nerve transection [74]. This outcome is a limitation of the current study's design, namely the complete neurectomy used to create the RPNIs. Future work could focus on the construction and evaluation of RPNIs using only partial neurectomies and reinnervation of muscle grafts with only certain nerve fascicles rather than whole nerve, so as to preserve as much muscle and nerve function as possible yet make available an RPNI signal.

3.4.5   RPNI Signal Period Co-varies with Gait Period

For all 10 bouts of walking data from the RPNI rats, with each bout containing 4 continuous walking steps at a relatively constant speed, the power spectrum of the RPNI signal produced a strong spectral component at around 2 Hz, which matched the chief component found in the power spectrum of the signals from the kinematic analysis (Figures 3.8 and 3.9). The same analysis applied to walking bouts from a rat walking at a higher speed produced a chief spectral component

at a frequency elevated by the same amount in both the RPNI and kinematic recordings. That is, variation in the fundamental frequency that appeared as the rat sped up and slowed down their walking (with corresponding movement forward and backward in each camera frame) could be found in both the RPNI and kinematic signals. This finding can also be used to support the claim that the RPNI signal is centrally generated.

When the strides are time-course averaged (time-warped to align footfall events and averaged at each timestep), a clear pattern emerges in the signals for both the Control and RPNI groups. Figure 3.6 shows the time-course averaged kinematics and Figure 3.7 shows the time-course averaged EMG signals. The emergence of these patterns is of course another reflection of the periodicity in the signals. Closer inspection of the patterns shows differences between the right and left hind limbs, as expected (Figure 3.7). But again, the kinematic and EMG signal patterns differ for the same leg between the RPNI and Control groups.

3.4.6 Decoder Performance

The altered gait observed between Control and RPNI rats was evidently accompanied by altered neural firing patterns. If the underlying neural firing patterns differ between the RPNI and Control groups, then the utility in comparing EMG signals across groups is for the most part lost. However, a decoder can be used to make within-group comparisons and to develop a common metric for each experimental group. I thus built a linear decoder that predicted ankle joint kinematics using 20 copies (at increasing delays) of the EMG signal for the corresponding rat. Half of the kinematic and EMG data were used to construct the decoder (derive a regressor matrix) while the other half were used to test the decoder. I used the Coefficient of Determination and Standard Error of the Estimate to quantify the dependence of ankle joint position on the EMG-derived kinematics. These model fitting metrics indicated that approximately 83% of the ankle kinematic variability for the left and right legs of RPNI rats can be attributed to the myoelectric signals obtained from the construct. By comparison, EMG data obtained from control rats accounts for 90% of the variability in ankle kinematics.

3.4.7 Potential for Human Use

The RPNI is intended as a means to transduce signals suitable for prosthesis control from the peripheral nerves of an amputee who lacks the muscles originally innervated by that nerve. As in TMR, a surgical intervention would be used to create RPNIs in humans, though RPNIs would involve the reinnervation of autologous grafted muscle and the placement of intramuscular or epimysial electrodes. The study presented here was intended to establish feasibility of the RPNI approach by recording from awake ambulating rats. The promise of RPNIs to offer many control

channels in humans because of their relatively small size and preparation with nerves that have been divided down to individual fascicles will need to be studied in follow-on studies that support translation to humans.

3.5   Conclusion

In vivo myoelectric RPNI activity is periodic. Contamination from muscles adjacent to the RPNI is minimal, as demonstrated by the results obtained from the Denervated group. The strong bilateral correlation and periodicity obtained between the EMG signals from an RPNI and the ankle joint motion indicates that the RPNI produces a reading of activity on its associated peripheral nerve. Together with the histological evidence collected to date, the results from the present chapter indicate the viability of the RPNI as a transducer for signals on peripheral nerves.

<center>**CHAPTER 4**</center>

Adjacent Regenerative Peripheral Nerve Interfaces Produce Phase-Antagonist Signals during Voluntary Walking in Rats

4.1   Introduction

Acquiring a sufficient number of independent peripheral nerve signals from an amputee's residual limb is critical to the control of an advanced prosthetic device. And despite the existence of sophisticated multiple DOF prosthetic devices, implementation has been limited as the search continues for an optimal interface between human and prosthesis [75]. TMR, which employs nerve transfers to reinnervate specific muscle sites, is the most immediately applicable interfacing strategy that has been demonstrated to provide neural input signals for prosthetic control [28]. Other strategies include direct brain interfaces, which have also been successfully tested in humans, but are generally considered too invasive and high-risk for a population of patients with limb loss [76]. Peripheral nerve interfaces involving epineural and intraneural electrodes have been studied as well [77], but the pNG signals acquired are small and likely subject to degeneration over time [59].

An alternative interface currently under development is the RPNI, which uses a muscle graft to interface between a severed nerve and the electronics of a prosthetic device [78]. Specifically, an RPNI device consists of a nonvascularized skeletal muscle graft that is implanted with, and subsequently neurotized by a transected peripheral nerve. Through the muscle graft, nerve signals can be transmitted, amplified, and detected by either epimysial or intramuscular electrodes [61]. Unlike TMR, the RPNI is not restricted to the utilization of vascularized muscle within the residual limb or the nearby chest wall, thereby permitting physiologically relevant connections to individually functioning fascicles within the peripheral nerve. The small size of the RPNI holds promise for the placement of multiple such constructs in a confined space such as the forearm. Furthermore, by connecting the severed nerve to a muscle graft, the RPNI also prevents neuroma formation.

Previous studies performed in anesthetized rats have shown the feasibility and durability of the

<center>50</center>

RPNI construct [61–63, 67–70]. Investigation of RPNI function in awake, walking rats demonstrated that in vivo myoelectric RPNI activity is periodic and entrained with gait, with signal amplitudes similar to controls, and minimal signal contamination from muscles adjacent to the RPNI [79]. While this study demonstrated the viability of the RPNI as a transducer for signals on peripheral nerves during rodent walking, it did not assess the performance of multiple adjacent RPNIs.

This chapter examines the potential for creating multiple adjacent RPNIs in the same limb, with the signals of each construct encoding a different function. The RPNI is created with fascicles of peripheral nerves known to function as antagonist pairs during voluntary hind limb locomotion. RPNI signals are acquired from 2 rats, and compared to signals obtained from similarly functioning muscles of 2 Control rats during treadmill walking. The main performance metrics for RPNI characterization are signal amplitude and signal correlation with hind limb joint kinematics. I expect antagonist pair signal activation from the RPNIs similar in amplitude and function to Controls.

4.2   Materials and Methods

Four male 3-month-old F344 strain rats were used in this study. All animal care and use procedures were conducted in accordance with the National Research Council's *Guide for the Care and Use of Laboratory Animals* (1996) and were approved by the University of Michigan Animal Care and Use Committee.

4.2.1   Surgical Preparation

Two Dual-RPNI group rats received a free right TA muscle transfer, and a free right EDL muscle transfer to the right thigh. Both muscles were sutured adjacent to the femur. The TA was neurotized with the proximal end of the transected peroneal nerve, while the EDL was neurotized with a fascicle of the tibial nerve, transected from one head of the gastrocnemius muscle. The remainder of the tibial nerve was left intact, so as to provide innervation to the posterior compartment of the lower hind limb. Each muscle was equipped with a bipolar patch electrode. Two Control group rats, in which the neuromuscular anatomy remained intact, received two bipolar patch electrodes, one on the right soleus and another on the extensor digitorum longus (EDL) muscles. In both groups, the bipolar patch electrodes (Double Standard, EP203 Customized; Microprobes, Gaithersburg, MD) were sutured to the respective muscles epimysium. The patch consisted of Teflon® insulated fine stranded stainless steel leads embedded in Dacron® reinforced silicone rubber, 0.18 mm thick. A piece of decellularized small intestinal submucosa (Surgisis, Cook Biotech,

West Lafayette, IN) was trimmed to size, hydrated, sterilized with 70% alcohol, rinsed, and then wrapped around each muscle-electrode unit to secure the electrodes in place. The cables from the electrodes were tunneled subcutaneously and secured to a head cap that was fixed to the skull using cortical screws and methyl methacrylate (Sigma-Aldrich, Co. LLC, St. Louis, MO). The surgical sites were then closed with suture (Figure 4.1).
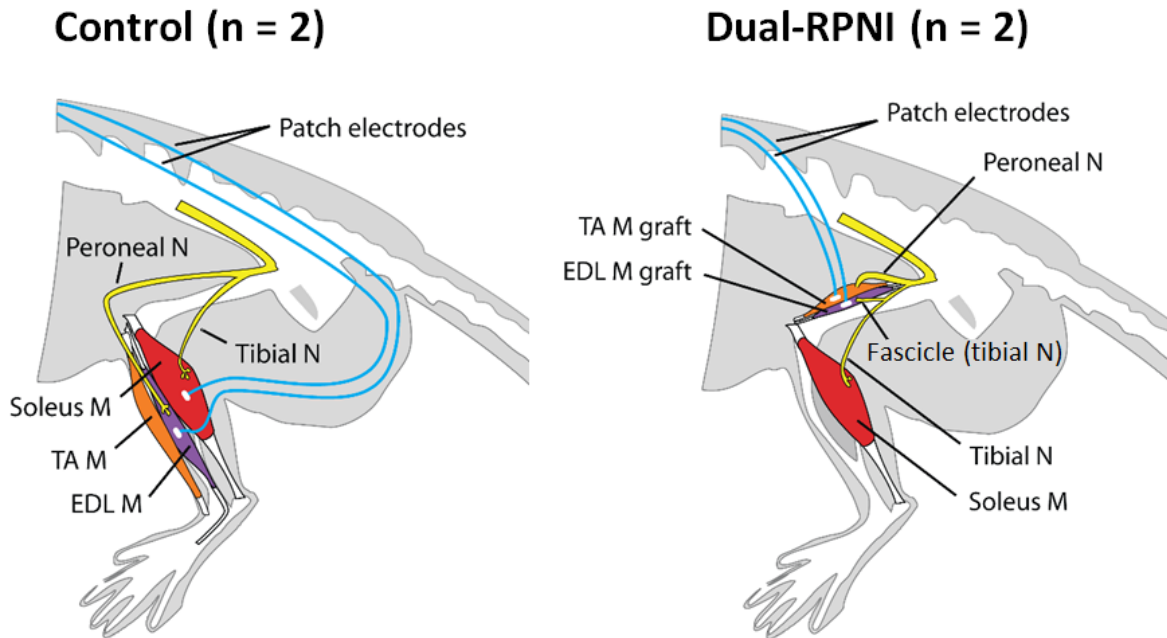
Figure 4.1: Schematic Diagram of the right hind limbs, indicating nerves, muscles, and bipolar electrode placement for the Control and Dual-RPNI study groups. The only surgical intervention for rats in the Control group involved electrode placement. Rats in the Dual-RPNI group underwent a free EDL muscle transfer with placement of a fascicle of the tibial nerve, and a free tibialis anterior muscle transfer with placement of the peroneal nerve. Both muscle transfers were placed adjacent to one another, and anchored to the femur in the right hind limb. Abbreviations: M = muscle; N = nerve.

Each rat recuperated for 4 months to facilitate wound healing and, for the Dual-RPNI group, reinnervation of the free muscle grafts. On the day of an evaluation (within the fourth month after surgery), each rat's right hind limb was shaved; on the bare skin, non-toxic clay based paints were used to mark the positions of the hip, knee, and ankle joints, as well as the distal end of the paw. Wire electrode ends were accessed through the head cap and connected to the EMG recording apparatus.

4.2.2   Recording Apparatus

Rats were conditioned to walk on a rat treadmill (Columbus Instruments, Columbus OH) at constant pace between 8.5 and 9.0 m/min. One high speed camera capable of recording at 120 frames per second (GoPro Hero2, San Mateo, CA) was positioned with its field of view perpendicular to the rat's walking direction and activated through a digital trigger. Myoelectric signals were amplified and bandpass filtered (1-500 Hz) with the use of a custom-built analog bipolar instrumentation amplifier. A nominal gain of 1000x was used and signal amplitudes were calibrated using a function generator and oscilloscope. The amplified and filtered signal was acquired at a 3 kHz sampling rate; during post-processing, it was digitally rectified and zero-phase low-pass filtered to 50 Hz. An LED positioned within the field of the camera was toggled off and on through a button press. The LED control signal was recorded by the data acquisition system to facilitate synchronization between the video and myoelectric recordings.

A custom video and data processing program was written in MATLAB (Mathworks, Natick, MA) to facilitate synchronization of the video and myoelectric recordings and extraction of hind limb kinematics from the video. The LED appearing in the video enabled the motion recordings to be synchronized to the LED control signal recorded alongside the myoelectric signals. Within the video processing program, a computer vision algorithm was written in MATLAB to extract centroid locations for each of the right hip, knee, ankle, and toe color markers appearing in each frame of the video recordings. These centroid locations were used in turn to identify hip, knee, ankle and toe joint angle trajectories of the right hind limb.

The identified centroids and limb segments were displayed in overlay on the video recordings. The visualization program's user interface supported the addition of gait event markers to the dataset. Gait events indicating right paw landing and lift-off were added to each dataset, allowing the categorization of the gait data into periods of stance (landing to lift-off) and swing (lift-off to landing).

The extracted kinematic and EMG data was divided into bouts, wherein each bout contained data for four or more complete strides. Walking was defined as a bout during which one or the other hind limbs was in contact with the treadmill belt. Sequences in which the rat was standing still or hopping were removed. This data was used to assess instantaneous EMG signal strength during walking cycles, and assess the cross-correlation between ankle joint kinematics and EMG data during stance and swing phases of gait.

4.2.3   Data Analysis

To assess myoelectric signal strength from all groups, the area under the curve of the filtered EMG data collected during the walking trials was calculated. These data were then segmented

into stance and swing and normalized across the gait period. Paired two-sample t-Tests were used to statistically differentiate between EMG activity values obtained from each group, using PASW Statistics 22, (SPSS, IBM Inc., 2013, Armonk, NY). The EMG activity resulting from each muscle was analyzed separately.

For the purpose of comparing kinematic and EMG data between groups for an average step, right hind paw gait events were used to segment the kinematic and EMG recordings into stance and swing phases of gait for each leg. Stance was defined between the hind paw making contact with the treadmill (landing) and subsequent liftoff. Swing was defined between liftoff and the next landing event. Each gait cycle (including kinematic and myoelectric recordings) was time-course normalized such that the beginning of stance corresponded to 0% and end of swing corresponded to 100% of gait for either hind limb. Within each experimental group, normalized kinematic and myoelectric recordings were aligned using the landing gait events before being used to compute a mean and standard deviation representative of a single step for all joint angles and EMG data.

4.3   Results

Raw EMG signals were more active with higher amplitudes during walking sequences than during periods of standing still in both Control and Dual-RPNI rats. EMG signals from both of the Control and both of the Dual-RPNI rats exhibited an alternating pattern of activity during continuous walking. Figure 4.2 shows representative ankle joint kinematics and raw EMG activity from the two adjacent constructs in an RPNI rat during five consecutive steps. The time axis is labeled according to whether the hind limb was in the stance or swing phase. In particular, the signals recorded from both RPNIs during walking featured large excursions with peak to peak voltage amplitudes ranging between 0.75 to 1.0 mV_{PP}. These voltage peaks occurred during different points in the gait cycle for each RPNI.

Walking EMG signal strength for each experimental group was quantified by integration of the area under the curve of the filtered EMG traces obtained per stride. Figure 4.3 illustrates the myoelectric activity (depicted as percent activity during stride) transduced from the tibial (top) and peroneal nerve (bottom) signals of the Control (left) and Dual-RPNI rats (right) during 32 walking steps. Comparison between the signals transduced from similar nerves shows matching activity profiles in Control and Dual-RPNI rats during stance and swing.

Paired two-sample t-Test comparisons were made between the mean EMG signal activity obtained from Control rats. A similar comparison was performed for the Dual-RPNI EMG data. Figure 4.4 presents the mean and standard deviation of the EMG activity obtained from the Control and Dual-RPNI group rats during walking. Within-group comparisons of Control and Dual-RPNI
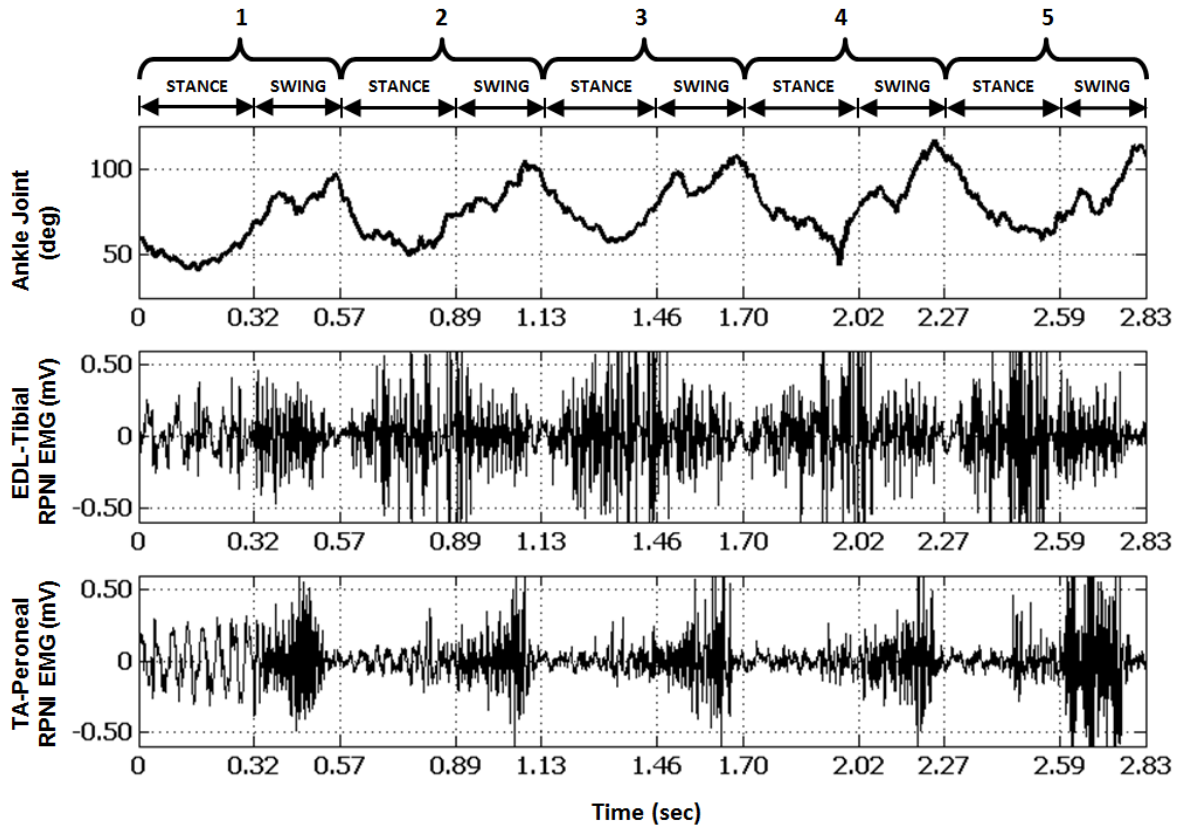
Figure 4.2: Ankle kinematic (top) and myoelectric data (center, bottom) obtained from the right hind limb of a Dual-RPNI rat, equipped with two adjacently placed RPNI interfaces during five consecutive steps of a walking task. The time periods are labeled according to whether the hind limb was in the stance or swing phase.

signals demonstrate a significant difference $(p < 0.01)$ between the EMG activity transduced from the tibial and peroneal nerves in either group.

The EMG signal patterns extracted from the video recordings during 32 strides from the 2 Control and 2 Dual-RPNI rats were normalized in time to align foot landing events. Within study groups, these signals differed as a function of the nerve from which they originated. Between groups, similar nerves produced comparable EMG traces. In particular, the EMG signal transduced from the tibial nerve in both groups demonstrated more activity during the stance phase, when hind limb plantar-flexion is most pronounced. Peroneal nerve activity was increased during swing, when paw liftoff occurs via dorsi-flexion. Figure 4.5 depicts the time course averaged EMG signal obtained from the musculature innervated with the tibial nerve (red) and peroneal nerve (purple) of Control rats (left) and Dual-RPNI rats (right). Shaded regions behind the average trace indicate one standard deviation.
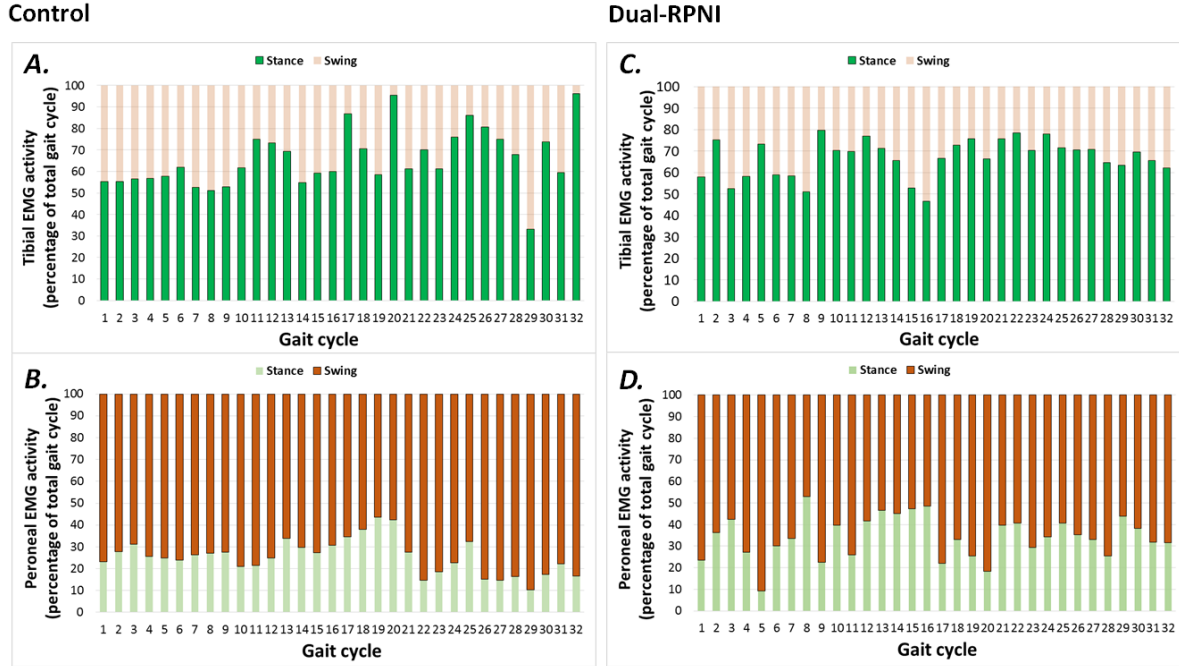
Control   **Dual-RPNI**

Figure 4.3: EMG signal activity, illustrated as a percentage of the total gait cycle obtained from the musculature of 2 Control group rats (left) and 2 Dual-RPNI group rats (right) during 32 strides. Activity transduced from **A.** tibial nerve (Control), **B.** peroneal nerve (Control), **C.** tibial nerve (Dual-RPNI) and **D.** peroneal nerve (Dual-RPNI) has been segmented into stance and swing for each step.

4.4 Discussion

This chapter explores an important obstacle that must be addressed in the quest for high-fidelity signal acquisition required for voluntary prosthetic control by humans using RPNI constructs. Achievement of *intuitive* prosthetic control requires that for each DOF, antagonist-pair RPNIs transduce signals similar to their antagonist-paired anatomic counterparts. The previous work with single bilateral RPNIs (presented in Chapter 3) indicated that signals from RPNIs consistently exhibited amplitudes similar to myoelectric signals acquired from analogous muscles in control rats [79]. Furthermore, RPNI function was not corrupted by the presence of motion artifact or simultaneously contracting muscles, and was highly correlated with a walking task. These findings were promising, as implementation of RPNI constructs in a limb places them in the vicinity of simultaneously contracting muscles, whose surgical excision is not an option, and whose presence must not affect the RPNI's output.

However, in that previous investigation, the use of whole peripheral nerves to create bilateral
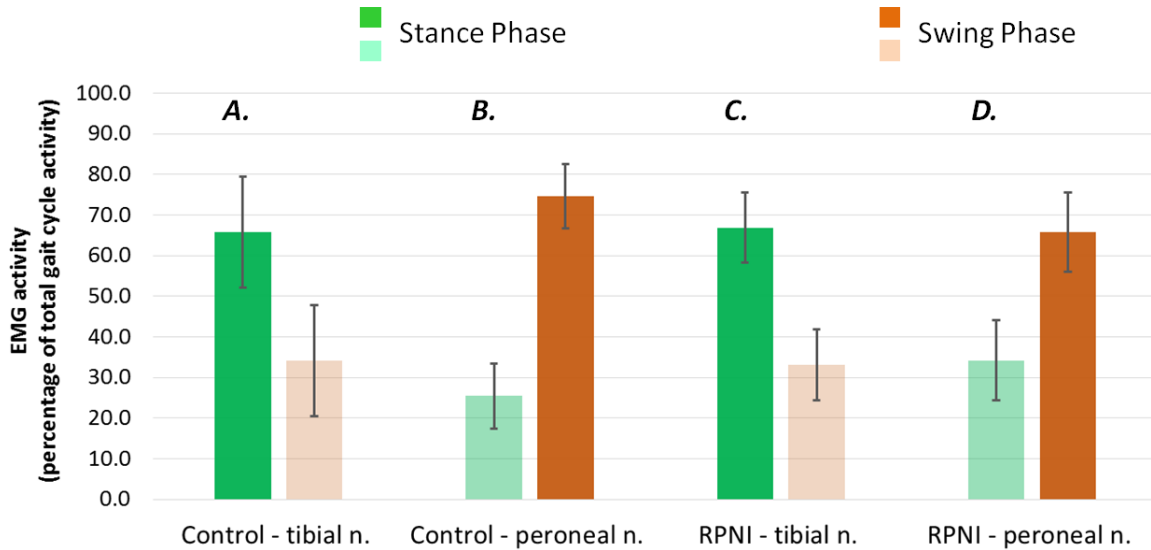
Figure 4.4: Mean ± one standard deviation of EMG signal activity obtained during stance and swing, illustrated as a percentage of the total gait cycle obtained from **A.** tibial nerve (Control), **B.** peroneal nerve (Control), **C.** tibial nerve (Dual-RPNI) and **D.** peroneal nerve (Dual-RPNI).
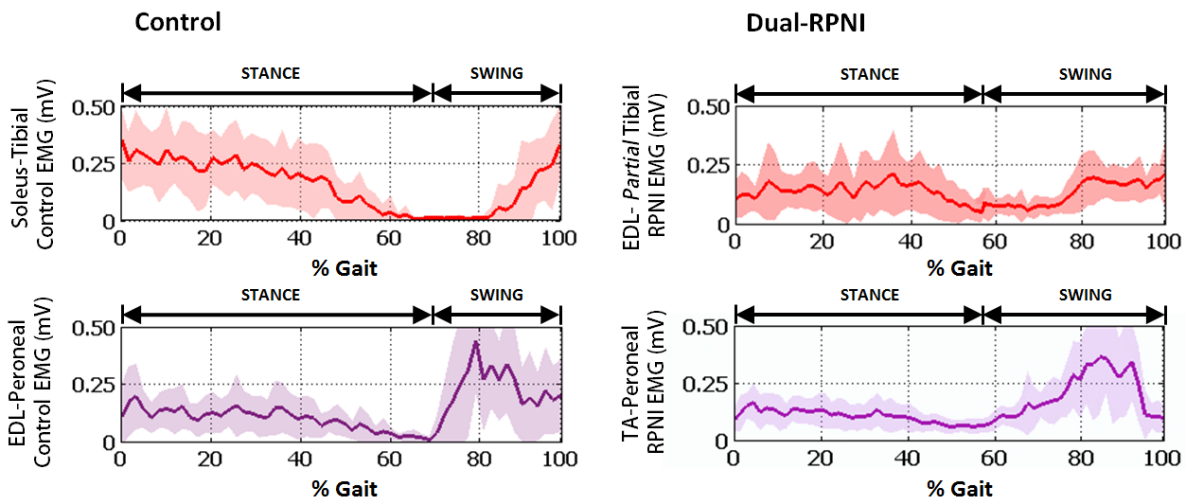
Figure 4.5: Time course average and standard deviation of 32 EMG signals, obtained from the musculature innervated with the tibial nerve (red) and peroneal nerve (purple) of 2 Control rats (left) and 2 Dual-RPNI rats (right) during walking. Traces have been normalized with respect to gait cycle, and separated into the stance and swing phases of gait.

RPNIs in the rat hind limbs resulted in a marked gait alteration, and may explain the significantly different EMG activity profile demonstrated by the RPNIs, especially in the tibial nerve construct

whose function during gait stance plantar-flexion is essential. To address this finding, and further characterize RPNI function, the study reported here has four new features. In particular this study: (1) employed RPNI constructs reinnervated with nerves known to exhibit antagonist activation, (2) placed RPNI constructs in proximity to one another, (3) used a fascicle (instead of the whole) tibial nerve to create an RPNI, and (4) harvested muscle grafts associated with different peripheral nerves than the ones used in the RPNIs.

Outcomes from features (1) and (2) of the present study demonstrated that RPNIs are capable of transducing the same out of phase neural signals as antagonist muscles mechanically doing work about a joint. This finding is illustrated as percent EMG activity as a function of gait phase in Figure 4.4, and time course normalized traces in Figure 4.5. The similarity of the activity profiles of these signals to controls demonstrates that adjacently placed RPNIs are not affected by crosstalk between constructs. This finding corroborates the observation from the previous work described in Chapter 3, that RPNIs are not sensitive to noise emanating from adjacent contracting musculature. The results obtained from study feature (3) are equally promising. In particular, use of a nerve fascicle to reinnervate a muscle graft of different innervation origin suggests that subsets of peripheral nerves can be used to create differently functioning RPNIs, or left in place to maintain innervation of existing musculature. The latter may be particularly important, as it resulted in the preservation of gait in a rat hind limb model. Moreover, results pertaining to study feature (4) sustain the idea that RPNIs can be created from multiple kinds of skeletal muscle tissue with no loss of function. This is particularly meaningful, as reconstructive surgical operations frequently make use of muscle grafts harvested from different parts of the body, where their function is either redundant, or not essential for most activities of daily living.

4.5   Conclusion

Adjacently placed RPNIs reinnervated with nerves exhibiting antagonist-pair function provide out-of-phase trajectories similar in amplitude and activity to Controls. Placement of RPNI constructs in proximity to one another does not lead to crosstalk. Use of peripheral nerve fascicles instead of whole nerve does not alter RPNI function, and use of fascicles to reinnervate RPNI constructs may provide the advantage of transducing multiple independent signals for increased DOF control in a prosthesis. Moreover, muscle isografts of different innervation origin may be used to construct an RPNI, with no negative effects on its function. These findings suggest that adjacently paired RPNI control sites may yield improved multi-DOF fidelity for upper limb amputees utilizing a motorized prosthetic device.

CHAPTER 5

Conclusions and Future Work

5.1 Epilogue

Compacting the description of a system into a model yields some noteworthy trade-offs. Advantages include the ability to develop analytical tools which focus on the most important system components affecting the studied output(s), and isolating the most influential inputs and states governing the system's behavior under a limited set of operating conditions. In such a limiting environment, the effect of disturbances, or exogenous signals which cannot be manipulated, can also be analyzed. The principal disadvantage of system simplification is twofold. First, any model, regardless of complexity, is an estimation of the entity being studied, and thus, no model can fully capture the behavior of a system in the real world. Second, estimation of a system produces some amount of uncertainty, part of which is a limitation of the noise inherent to all sensors, and part of which is a consequence of the inability to account for all of the variables that influence system performance. To some extent, both of these disadvantages can be alleviated (though not completely eliminated) by the use of more sophisticated and reliable sensors, but more importantly, by careful experimental design, and by an understanding of when to apply the medical or engineer's definition of *system* to the research topic being addressed.

5.1.1 Chapter 2: Training Surgical Skills

An increased emphasis on competency based medical education [80, 81] has driven the development of training techniques that employ quantifiable metrics to measure performance [82, 83] and assessment tools to measure trainees' attainment of proficiency within these defined domains [82, 84, 85]. Incorporating immediate, valid feedback into deliberate training is needed for trainees to gain expertise as they work toward proficiency [84, 86], and robust, valid assessment tools will often serve as a source for this important feedback. The stringent reality of today's operating room environment can limit trainees' opportunities for hands-on practice and feedback in the operating room [82, 87]; these constraints, coupled with the reduction in resident duty hours, have created

the need for contemporary surgical training curricula that emphasize deliberate practice with feedback, ideally prior to application in patients [82]. Criterion-based curricula, which allow trainees to focus on specific skills, with repeated practice and immediate feedback, allow for the development of a "pretrained novice" prior to his or her performing in the operating room [86].

Early efforts to develop competency based curricula in surgical education lost momentum in the 1970s and 1980s in part because of the lack of adequate assessment tools [88]. Renewed emphasis on competency based assessment in the last decade has led to the development of guidelines for robust tools to assess competency within clinical educational settings. These guidelines recommended that assessment tools be feasible and provide valid, reliable, and useful data [85]. Whereas structure and process-based assessments rely primarily on single subjective measures, such as overall performance of a trainee, competency based assessments require the use of multiple objective measures [88, 89].

In criterion-based training, objective assessment of performance provides essential feedback by identifying when and to what degree a trainee deviates from an established standard or expectation. This objective feedback may contribute to efficient practice and may lead to greater competency [82, 84, 86]. Established assessments, such as the objective structured clinical examination and the objective structured assessment of technical skills, rely on structured observation with defined criteria and demonstrate good validity and reliability [82, 85].

Whether educators perform these observations in a clinical or simulated environment, they require significant time and effort by an evaluator who is trained both in the clinical skill being assessed and in how to use the assessment tool. Emerging technologies, such as virtual reality simulators and motion-tracking devices, are also valid assessment tools for technical skills in some instances and may require less of a commitment from the evaluator; however, they have other limitations [82, 85]. For example, motion-tracking assessment tools discriminate between early training levels by measuring motion efficiency, but they do not allow for more granular feedback about trainees' performance or end-product quality [90]. Thus, a trainee could become very efficient at completing a task, scoring well on the motion-tracking assessment, but the quality of his or her end product may be poor because only the efficiency of his or her motion is tracked and reported.

Given these observations, the prototyping of a surgical trainer capable of providing the resident-in-training with objective feedback that can be translated into improved outcomes in the operating room is prescient. This is especially important given that, as the computational model of abdominal fascia closure from Chapter 2 illustrates, correct tensioning of a sutured abdominal closure is not straightforward. It is different than placement and must have a certain concave profile to provide wound edge apposition. Thus, tension feedback is necessary along with proper suture placement feedback.

Rather than employing a performance based approach to this problem, which would require the modeling and characterization of the complex kinematics of the human arm (whose axis of rotation changes as it progresses from pronation to supination) and needle trajectory as it drives suture through the abdominal fascia, a results based modelling approach was devised. This approach is simpler to model, as the only model required is a computational one capable of measuring the forces required to appose the abdominal fascia edges via tissue mechanics. By only focusing on the results of the procedure, freedom is provided to analyze specific parameters of suture placement and tension in order to assess what creates the optimal closure, (i.e. there may be more than one set of kinematic parameters for the human arm and needle to obtain the same suture placement and tension).

This approach also allows the creation of a surgical trainer capable of monitoring suture tension and placement, and a set of performance and product feedback which can intuitively guide the user towards optimal suturing technique. To date, this work has demonstrated good agreement between the physical and virtual (FE) neoprene models under various loading and stretching conditions via the superposition of the dotted grids, using a method akin to digital image correlation techniques. Based on these promising results, future work envisions the validation of the suture tension estimates provided by the FE model via instrumentation capable of measuring suture tension on the physical neoprene closure [91]. This would allow the use of the FE model in conjunction with the physical model to estimate the suture tension in a physically simulated abdominal closure via the alignment of the virtual and physical dotted grids. It is hoped that with the starting basis of the surgical trainer and feedback already designed, future assessments of abdominal closures using medical students and surgical residents can inform the best visual means of providing suture tension and placement feedback. Assessments of performance and learning effects from a repeated measures human subject study would reflect whether such feedback is instructive and helpful, and would be the final step in the development of a commercially viable surgical trainer prototype designed to provide a better means of communicating the directives required for proper suturing performance to medical personnel in training.

5.1.2 Chapter 3: In Vivo Function of a Neuromuscular Interface

The RPNI is based on many years of research in muscle physiology and regenerative medicine, much of which was pioneered in the Neuromuscular Lab at UM. This body of work, dating back to 1989 [92], and predated by the work of others since the early 1970s, describe experiments characterizing the viability and structure of reinnervated muscle (both free and fully vascularized). In particular, the effect of delayed reinnervation on the function and mass of vascularized muscle isografts is described in [93]. Reference [94] provides concise histological evidence that reinner-

vation of a muscle graft supports muscle regeneration via quiescent satellite cell proliferation and fusion which leads to formation of new muscle fibers from multinucleated myotube precursors. This work has been followed up with an assessment of muscle structure and contractile function following two episodes of denervation [95], as well as an investigation into the use of nerve grafts maintained viable by insertion into a donor innervated muscle, for later reinnervation of denervated muscles when acute primary epineural repair is not feasible [65]. Finally, all of the findings regarding the effects of reinnervation on muscle regeneration and function are presented as a best practices article on the subject of optimizing skeletal muscle reinnervation and maximizing muscle graft regeneration [96].

At the time I began work in the Neuromuscular Lab, knowledge of RPNI function was based on studies conducted in rats under anaesthesia and on histological studies. Stimulation of proximal nerve in anaesthetized rats was known to produce CMAPs and muscle force transients. These signals were easily acquired by epimysial electrodes that could potentially be deployed as permanent implants, but results involving implanted electrodes were not yet available. More importantly, the promise of the RPNI to transduce signals generated by the rat CNS had not been established since experiments involving awake freely behaving rats had yet to be undertaken.

My work on the RPNI project is characteristically translational research: it was intended to support, in the most expeditious manner possible, translation of the RPNI technology from rats (and monkeys) into humans. A chief feature to be established for RPNI function is selectivity: do the signals from one or more RPNI prepared in the rat encode the intended motor function of the rat CNS and do they do independently? Naturally, motor function is expected to derive from the particular nerve innervating a given sample of muscle tissue. Muscle tissue is in fact generic. It derives its mechanical function from its attachments to the skeletal system but derives its activation function (timing, selection, signaling function) from the nerve that innervates it. Note that the generic nature of muscle and specific signaling function of nerve is also the basis of TMR.

My acumen both as an engineering researcher and as a medical researcher have been exercised to their fullest and have grown substantially through my involvement in the RPNI project. While initially I was interested in creating what promised to be some very exciting demonstrations of RPNI function (that I called the Rat Chariot), I soon turned to translational research instead. The Rat Chariot, by the way, was a rat-sized differential-drive mobile robot upon which the rat would have ridden, with steering controlled by two RPNI signals. The Rat Chariot was valuable as an RPNI demonstrator, but not so much for its scientific advancement.

Instead, I collected RPNI signals from awake rats while they walked on a treadmill, using videography in addition to high-speed signal acquisition and real-time signal visualization of the RPNI signals. I investigated relationships between periodicity in the RPNI signals and kinematic data and conducted correlation analyses between the RPNI and kinematic signals.

While I was quite tempted to build a type of first principles model that would describe the relationship between RPNI signals and gait (based on biomechanics and muscle function modeling), I resorted instead to empirical models. The empirical models have in fact served the translational goals very well. The biomechanical models would have only raised more questions. My research was hypothesis-driven, to determine the function and limits of function of the RPNI and test, as best as could be expected in the rat, whether the RPNI signals encoded volitional motor commands of an awake rat. The ultimate objective was not to develop a model based on the motive function (preserved or lost) of individual muscles firing at certain times and acting on certain parts of the skeleton.

5.1.3   Chapter 4: In Vivo Function of Adjacent Neuromuscular Interfaces

The use of an empirical model to assess RPNI function proved once again beneficial in the evaluation of adjacently placed RPNI constructs reinnervated so as to encode antagonist pair function. The small size of the RPNI renders it feasible to place many such constructs in the vicinity of one another. Moreover, the use of fascicles to reinnervate the muscle grafts could allow the careful selection and transduction of neural signals to each DOF of a computerized prosthetic interface.

It has long been known that within a peripheral nerve, individual nerve fibers are grouped together in fascicles [97], and surgical procedures describing the dissection of peripheral nerves into distinct fascicular bundles are well established [98]. Clinical investigations have also demonstrated that somatotopic clustering of nerve fibers within the fascicular bundle persists for most of the nerve's length from the distal to its proximal end. In particular, neurophysiological research has shown that a high degree of somatotopic organization exists in the nerve fibers which constitute peripheral nerve fascicles [99]. This is in accord with the somatotopic organization known to exist for motor and sensory pathways in the CNS.

By employing a model of percent signal activity during each gait of a walking task, this work demonstrated that adjacent RPNIs neurotized with agonist/antagonist nerves activate independently during voluntary walking, with signal activity patterns similar to Controls. Moreover, RPNIs constructed with fascicles rather than whole nerves and isografts of any musculo-motor origin function in vivo similar to Controls. This successful evaluation of RPNIs reinnervated with fascicles shows promise towards the creation of multiple constructs, each with a well defined function providing a unique signal to one DOF in a computerized prosthetic device.

5.1.4   Addendum

The famous statistician George E. P. Box is credited with stating that "all models are wrong, but some models are useful." [100] The bodies of work which factor into this dissertation are testament

to the prescience of designating which system models are appropriate in the pursuit of the fruition of translational research in the fields of medicine and engineering.

BIBLIOGRAPHY

[1] B. F. Miller, ed., *Encyclopedia & dictionary of medicine, nursing, and allied health.* Philadelphia: Saunders, 7th ed ed., 2003.

[2] K. J. Keesman, *System identification: an introduction.* Advanced textbooks in control and signal processing, London ; New York: Springer, 2011.

[3] L. A. Israelsson, T. Jonsson, and A. Knutsson, "Suture technique and wound healing in midline laparotomy incisions," *The European Journal of Surgery = Acta Chirurgica*, vol. 162, pp. 605–609, Aug. 1996.

[4] H. Delingette, "Toward realistic soft-tissue modeling in medical simulation," *Proceedings of the IEEE*, vol. 86, pp. 512–523, Mar. 1998.

[5] H. Delingette and N. Ayache, "Hepatic surgery simulation," *Communications of the ACM*, vol. 48, p. 31, Feb. 2005.

[6] A. Okamura, C. Simone, and M. O'Leary, "Force Modeling for Needle Insertion Into Soft Tissue," *IEEE Transactions on Biomedical Engineering*, vol. 51, pp. 1707–1716, Oct. 2004.

[7] M. Mahvash and P. Dupont, "Mechanics of Dynamic Needle Insertion into a Biological Material," *IEEE Transactions on Biomedical Engineering*, vol. 57, pp. 934–943, Apr. 2010.

[8] K. Miller and K. Chinzei, "Constitutive modelling of brain tissue: experiment and theory," *Journal of Biomechanics*, vol. 30, pp. 1115–1121, Dec. 1997.

[9] M. Farshad, M. Barbezat, P. Flüeler, F. Schmidlin, P. Graber, and P. Niederer, "Material characterization of the pig kidney in relation with the biomechanical analysis of renal trauma," *Journal of Biomechanics*, vol. 32, pp. 417–425, Apr. 1999.

[10] T. Hu and J. P. Desai, "Characterization of Soft-Tissue Material Properties: Large Deformation Analysis," in *Medical Simulation* (T. Kanade, J. Kittler, J. M. Kleinberg, F. Mattern, J. C. Mitchell, M. Naor, O. Nierstrasz, C. Pandu Rangan, B. Steffen, M. Sudan, D. Terzopoulos, D. Tygar, M. Y. Vardi, G. Weikum, S. Cotin, and D. Metaxas, eds.), vol. 3078, pp. 28–37, Berlin, Heidelberg: Springer Berlin Heidelberg, 2004.

[11] H. Saraf, K. T. Ramesh, A. M. Lennon, A. C. Merkle, and J. C. Roberts, "Measurement of the Dynamic Bulk and Shear Response of Soft Human Tissues," *Experimental Mechanics*, vol. 47, pp. 439–449, May 2007.

[12] S. DiMaio and S. Salcudean, "Interactive Simulation of Needle Insertion Models," *IEEE Transactions on Biomedical Engineering*, vol. 52, pp. 1167–1179, July 2005.

[13] F. Wang, E. Su, E. Burdet, and H. Bleuler, "Development of a microsurgery training system," *Conference Proceedings: ... Annual International Conference of the IEEE Engineering in Medicine and Biology Society. IEEE Engineering in Medicine and Biology Society. Conference*, vol. 2008, pp. 1935–1938, 2008.

[14] K.-S. Choi, S.-H. Chan, and W.-M. Pang, "Virtual Suturing Simulation Based on Commodity Physics Engine for Medical Learning," *Journal of Medical Systems*, Dec. 2010.

[15] S. F. Johnsen, Z. A. Taylor, L. Han, Y. Hu, M. J. Clarkson, D. J. Hawkes, and S. Ourselin, "Detection and modelling of contacts in explicit finite-element simulation of soft tissue biomechanics," *International Journal of Computer Assisted Radiology and Surgery*, vol. 10, pp. 1873–1891, Nov. 2015.

[16] K. Lister, Z. Gao, and J. P. Desai, "Real-time, haptics-enabled simulator for probing ex vivo liver tissue," *Conference proceedings: ... Annual International Conference of the IEEE Engineering in Medicine and Biology Society. IEEE Engineering in Medicine and Biology Society. Annual Conference*, vol. 2009, pp. 1196–1199, 2009.

[17] C. Sakezles, "Synthetic human tissue models can reduce the cost of device development," *Medical Device Technology*, vol. 20, pp. 32–34, Feb. 2009.

[18] G. Santhanam, S. I. Ryu, B. M. Yu, A. Afshar, and K. V. Shenoy, "A high-performance brain-computer interface," *Nature*, vol. 442, pp. 195–198, July 2006.

[19] J. L. Collinger, S. Foldes, T. M. Bruns, B. Wodlinger, R. Gaunt, and D. J. Weber, "Neuroprosthetic technology for individuals with spinal cord injury," *The Journal of Spinal Cord Medicine*, vol. 36, pp. 258–272, July 2013.

[20] R. A. Miranda, W. D. Casebeer, A. M. Hein, J. W. Judy, E. P. Krotkov, T. L. Laabs, J. E. Manzo, K. G. Pankratz, G. A. Pratt, J. C. Sanchez, D. J. Weber, T. L. Wheeler, and G. S. Ling, "DARPA-funded efforts in the development of novel brain–computer interface technologies," *Journal of Neuroscience Methods*, vol. 244, pp. 52–67, Apr. 2015.

[21] G. E. Loeb and R. A. Peck, "Cuff electrodes for chronic stimulation and recording of peripheral nerve activity," *Journal of Neuroscience Methods*, vol. 64, pp. 95–103, Jan. 1996.

[22] R. K. Gore, Y. Choi, R. Bellamkonda, and A. English, "Functional recordings from awake, behaving rodents through a microchannel based regenerative neural interface," *Journal of Neural Engineering*, vol. 12, p. 016017, Feb. 2015.

[23] T. Boretius, J. Badia, A. Pascual-Font, M. Schuettler, X. Navarro, K. Yoshida, and T. Stieglitz, "A transverse intrafascicular multichannel electrode (TIME) to interface with the peripheral nerve," *Biosensors & bioelectronics*, vol. 26, pp. 62–69, Sept. 2010.

[24] J. J. FitzGerald, N. Lago, S. Benmerah, J. Serra, C. P. Watling, R. E. Cameron, E. Tarte, S. P. Lacour, S. B. McMahon, and J. W. Fawcett, "A regenerative microchannel neural interface for recording from and stimulating peripheral axons in vivo," *Journal of Neural Engineering*, vol. 9, p. 016010, Feb. 2012.

[25] W. M. Grill, S. E. Norman, and R. V. Bellamkonda, "Implanted neural interfaces: biochallenges and engineered solutions," *Annual Review of Biomedical Engineering*, vol. 11, pp. 1–24, 2009.

[26] C. Welle and V. Krauthamer, "FDA regulation of invasive neural recording electrodes: a daunting task for medical innovators," *IEEE pulse*, vol. 3, pp. 37–41, Mar. 2012.

[27] G. McGimpsey and T. C. Bradford, "Limb prosthetics services and devices," 2008.

[28] T. A. Kuiken, "Targeted Muscle Reinnervation for Real-time Myoelectric Control of Multifunction Artificial Arms," *JAMA*, vol. 301, p. 619, Feb. 2009.

[29] K. Ohnishi, R. F. Weir, and T. A. Kuiken, "Neural machine interfaces for controlling multifunctional powered upper-limb prostheses," *Expert Review of Medical Devices*, vol. 4, pp. 43–53, Jan. 2007.

[30] P. Zhou, M. M. Lowery, K. B. Englehart, H. Huang, G. Li, L. Hargrove, J. P. A. Dewald, and T. A. Kuiken, "Decoding a new neural machine interface for control of artificial limbs," *Journal of Neurophysiology*, vol. 98, pp. 2974–2982, Nov. 2007.

[31] A. E. Schultz and T. A. Kuiken, "Neural interfaces for control of upper limb prostheses: the state of the art and future possibilities," *PM & R: the journal of injury, function, and rehabilitation*, vol. 3, pp. 55–67, Jan. 2011.

[32] J. W. A. Burger, J. F. Lange, J. A. Halm, G.-J. Kleinrensink, and H. Jeekel, "Incisional hernia: early complication of abdominal surgery," *World Journal of Surgery*, vol. 29, pp. 1608–1613, Dec. 2005.

[33] D. R. Flum, K. Horvath, and T. Koepsell, "Have outcomes of incisional hernia repair improved with time? A population-based analysis," *Annals of Surgery*, vol. 237, pp. 129–135, Jan. 2003.

[34] A. V. Pollock and M. Evans, "Early prediction of late incisional hernias," *The British Journal of Surgery*, vol. 76, pp. 953–954, Sept. 1989.

[35] "Advances in Wound Healing: A Review of Current Wound Healing Products," *Plastic Surgery International*, vol. 2012, 2012.

[36] R. J. Sanders and D. DiClementi, "Principles of abdominal wound closure. II. Prevention of wound dehiscence," *Archives of Surgery (Chicago, Ill.: 1960)*, vol. 112, pp. 1188–1191, Oct. 1977.

[37] D. Millbourn, Y. Cengiz, and L. A. Israelsson, "Effect of stitch length on wound complications after closure of midline incisions: a randomized controlled trial," *Archives of Surgery (Chicago, Ill.: 1960)*, vol. 144, pp. 1056–1059, Nov. 2009.

[38] T. T. Irvin, C. G. Koffman, and H. L. Duthie, "Layer closure of laparotomy wounds with absorbable and non-absorbable suture materials," *The British Journal of Surgery*, vol. 63, pp. 793–796, Oct. 1976.

[39] T. P. Jenkins, "Incisional hernia repair: a mechanical approach," *The British Journal of Surgery*, vol. 67, pp. 335–336, May 1980.

[40] H. Högström, U. Haglund, and B. Zederfeldt, "Suture technique and early breaking strength of intestinal anastomoses and laparotomy wounds," *Acta Chirurgica Scandinavica*, vol. 151, no. 5, pp. 441–443, 1985.

[41] D. J. Leaper, A. Allan, R. E. May, A. P. Corfield, and R. H. Kennedy, "Abdominal wound closure: a controlled trial of polyamide (nylon) and polydioxanone suture (PDS)," *Annals of the Royal College of Surgeons of England*, vol. 67, pp. 273–275, Sept. 1985.

[42] L. A. Israelsson and D. Millbourn, "Prevention of incisional hernias: how to close a midline incision," *The Surgical Clinics of North America*, vol. 93, pp. 1027–1040, Oct. 2013.

[43] P. Theocaris, D. Pazis, and B. Konstantellos, "The exact shape of a deformed internal slant crack under biaxial loading," *International Journal of Fracture*, vol. 30, no. 2, pp. 135–153, 1986.

[44] M. Singh, G. Glinka, and R. Dubey, "Notch and crack analysis as a moving boundary problem," *Engineering Fracture Mechanics*, vol. 47, pp. 479–492, Mar. 1994.

[45] R. N. Dubey, "Crack Induced Stress Field in an Elastic-Plastic Plate," in *Advances in Engineering Structures, Mechanics & Construction* (M. Pandey, W.-C. Xie, and L. Xu, eds.), vol. 140, pp. 493–504, Dordrecht: Springer Netherlands, 2006.

[46] Y. C. Fung, *Biomechanics: mechanical properties of living tissues*. New York: Springer-Verlag, 2nd ed ed., 1993.

[47] R. B. Martin, D. B. Burr, and N. A. Sharkey, *Skeletal tissue mechanics*. New York: Springer, 1998.

[48] M. Kirilova, S. Stoytchev, D. Pashkouleva, and V. Kavardzhikov, "Experimental study of the mechanical properties of human abdominal fascia," *Medical Engineering & Physics*, vol. 33, pp. 1–6, Jan. 2011.

[49] G.-R. Gillich, P. Bratu, D. Frunzaverde, D. Amariei, and V. Iancu, "Identifying mechanical characteristics of materials with non-linear behavior using statistical methods," in *Proceedings of the 4th WSEAS international conference on Computer engineering and applications*, (Cambridge, USA), pp. 96–103, World Scientific and Engineering Academy and Society (WSEAS), 2009.

[50] E. A. Biddiss and T. T. Chau, "Upper limb prosthesis use and abandonment: a survey of the last 25 years," *Prosthetics and Orthotics International*, vol. 31, pp. 236–257, Sept. 2007.

[51] Touch Bionics, " Ultra," 2014.

[52] RSLsteeper, "bebionic3 Technical information," May 2013.

[53] L. Resnik, S. L. Klinger, and K. Etter, "The DEKA Arm: its features, functionality, and evolution during the Veterans Affairs Study to optimize the DEKA Arm," *Prosthetics and Orthotics International*, vol. 38, pp. 492–504, Dec. 2014.

[54] M. S. Fifer, S. Acharya, H. L. Benz, M. Mollazadeh, N. E. Crone, and N. V. Thakor, "Toward Electrocorticographic Control of a Dexterous Upper Limb Prosthesis: Building Brain-Machine Interfaces," *IEEE Pulse*, vol. 3, pp. 38–42, Jan. 2012.

[55] A. Ameri, E. J. Scheme, E. N. Kamavuako, K. B. Englehart, and P. A. Parker, "Real-time, simultaneous myoelectric control using force and position-based training paradigms," *IEEE transactions on bio-medical engineering*, vol. 61, pp. 279–287, Feb. 2014.

[56] M. R. Wells, U. Vaidya, J. L. Ricci, and C. Christie, "A neuromuscular platform to extract electrophysiological signals from lesioned nerves: a technical note," *Journal of Rehabilitation Research and Development*, vol. 38, pp. 385–390, Aug. 2001.

[57] W. Truccolo, G. M. Friehs, J. P. Donoghue, and L. R. Hochberg, "Primary motor cortex tuning to intended movement kinematics in humans with tetraplegia," *The Journal of Neuroscience: The Official Journal of the Society for Neuroscience*, vol. 28, pp. 1163–1178, Jan. 2008.

[58] C. A. Chestek, V. Gilja, P. Nuyujukian, J. D. Foster, J. M. Fan, M. T. Kaufman, M. M. Churchland, Z. Rivera-Alvidrez, J. P. Cunningham, S. I. Ryu, and K. V. Shenoy, "Long-term stability of neural prosthetic control signals from silicon cortical arrays in rhesus macaque motor cortex," *Journal of neural engineering*, vol. 8, p. 045005, Aug. 2011.

[59] X. Navarro, T. B. Krueger, N. Lago, S. Micera, T. Stieglitz, and P. Dario, "A critical review of interfaces with the peripheral nervous system for the control of neuroprostheses and hybrid bionic systems," *Journal of the peripheral nervous system: JPNS*, vol. 10, pp. 229–258, Sept. 2005.

[60] T. A. Kuiken, A. E. S. Feuser, and A. K. Barlow, eds., *Targeted muscle reinnervation: a neural interface for artificial limbs*. No. 28 in Series in medical physics and biomedical engineering, Boca Raton: CRC Press, Taylor & Francis Group, 2013.

[61] T. A. Kung, N. B. Langhals, D. C. Martin, P. J. Johnson, P. S. Cederna, and M. G. Urbanchek, "Regenerative peripheral nerve interface viability and signal transduction with an implanted electrode," *Plastic and reconstructive surgery*, vol. 133, pp. 1380–1394, June 2014.

[62] Z. P. French, N. S. Carrothers, C. A. Hassett, J. D. Moon, N. B. Langhals, P. S. Cederna, and M. G. Urbanchek, "Abstract 61: Characterization of Regenerative Peripheral Nerve Device Signaling during Evoked Maximal and Submaximal Fatiguing Conditions," *Plastic and Reconstructive Surgery*, vol. 133, p. 72, Mar. 2014.

[63] N. B. Langhals, S. L. Woo, J. D. Moon, J. V. Larson, M. K. Leach, P. S. Cederna, and M. G. Urbanchek, "Electrically stimulated signals from a long-term Regenerative Peripheral Nerve Interface," *Conference proceedings: ... Annual International Conference of the IEEE Engineering in Medicine and Biology Society. IEEE Engineering in Medicine and Biology Society. Annual Conference*, vol. 2014, pp. 1989–1992, Aug. 2014.

[64] A. Nedic, D. Ursu, I. Sando, J. Moon, C. Hassett, R. B. Gillespie, N. Langhals, P. Cederna, and M. Urbanchek, "Abstract 16: Adjacent Antagonistic RPNIs Produce Independent Signaling for Prosthesis Control," *Plastic and Reconstructive Surgery*, vol. 135, p. 21, May 2015.

[65] M. G. Urbanchek, D. E. Ganz, M. A. Aydin, J. H. van der Meulen, and W. M. Kuzon, "Muscle-nerve-muscle neurotization for the reinnervation of denervated somatic muscle," *Neurological Research*, vol. 26, pp. 388–394, June 2004.

[66] M. G. Urbanchek, B. Wei, B. M. Egeland, M. R. Abidian, D. R. Kipke, and P. S. Cederna, "Microscale electrode implantation during nerve repair: effects on nerve morphology, electromyography, and recovery of muscle contractile function," *Plastic and Reconstructive Surgery*, vol. 128, pp. 270e–278e, Oct. 2011.

[67] Z. Baghmanli, K. B. Sugg, B. Wei, B. S. Shim, D. C. Martin, P. S. Cederna, and M. G. Urbanchek, "Biological and electrophysiologic effects of poly(3,4-ethylenedioxythiophene) on regenerating peripheral nerve fibers," *Plastic and Reconstructive Surgery*, vol. 132, pp. 374–385, Aug. 2013.

[68] I. C. Sando, M. K. Leach, S. L. Woo, J. D. Moon, P. S. Cederna, N. B. Langhals, and M. G. Urbanchek, "Regenerative Peripheral Nerve Interface for Prostheses Control: Electrode Comparison," *Journal of Reconstructive Microsurgery*, Oct. 2015.

[69] S. L. Woo, M. G. Urbanchek, M. K. Leach, J. D. Moon, P. Cederna, and N. B. Langhals, "Quantification of muscle-derived signal interference during monopolar needle electromyography of a peripheral nerve interface in the rat hind limb," *Conference proceedings: ... Annual International Conference of the IEEE Engineering in Medicine and Biology Society. IEEE Engineering in Medicine and Biology Society. Annual Conference*, vol. 2014, pp. 4382–4385, 2014.

[70] Y. Hu, I. C. Sando, P. S. Cederna, and M. G. Urbanchek, "Impact of Muscle Graft Volume on Signaling Capacity in the Regenerative Peripheral Nerve Interface for Neuroprosthetic Control," *Plastic and Reconstructive Surgery*, vol. 136, pp. 38–39, Oct. 2015.

[71] J. M. Carmena, M. A. Lebedev, R. E. Crist, J. E. O'Doherty, D. M. Santucci, D. F. Dimitrov, P. G. Patil, C. S. Henriquez, and M. A. L. Nicolelis, "Learning to control a brain-machine interface for reaching and grasping by primates," *PLoS biology*, vol. 1, p. E42, Nov. 2003.

[72] C. A. Chestek, A. P. Batista, G. Santhanam, B. M. Yu, A. Afshar, J. P. Cunningham, V. Gilja, S. I. Ryu, M. M. Churchland, and K. V. Shenoy, "Single-neuron stability during repeated reaching in macaque premotor cortex," *The Journal of Neuroscience: The Official Journal of the Society for Neuroscience*, vol. 27, pp. 10742–10750, Oct. 2007.

[73] A. K. Thota, S. C. Watson, E. Knapp, B. Thompson, and R. Jung, "Neuromechanical control of locomotion in the rat," *Journal of neurotrauma*, vol. 22, pp. 442–465, Apr. 2005.

[74] A. Gramsbergen, J. IJkema-Paassen, and M. Meek, "Sciatic Nerve Transection in the Adult Rat: Abnormal EMG Patterns during Locomotion by Aberrant Innervation of Hindleg Muscles," *Experimental Neurology*, vol. 161, pp. 183–193, Jan. 2000.

[75] J. V. Larson, T. A. Kung, P. S. Cederna, E. D. Sears, M. G. Urbanchek, and N. B. Langhals, "Clinical factors associated with replantation after traumatic major upper extremity amputation," *Plastic and Reconstructive Surgery*, vol. 132, pp. 911–919, Oct. 2013.

[76] P. G. Patil and D. A. Turner, "The development of brain-machine interface neuroprosthetic devices," *Neurotherapeutics: The Journal of the American Society for Experimental NeuroTherapeutics*, vol. 5, pp. 137–146, Jan. 2008.

[77] S. Micera, J. Carpaneto, and S. Raspopovic, "Control of Hand Prostheses Using Peripheral Information," *IEEE Reviews in Biomedical Engineering*, vol. 3, pp. 48–68, 2010.

[78] M. Urbanchek, Z. Baghmanli, B. Wei, B. Egeland, and P. Cederna, "155: LONG TERM STABILITY OF REGENERATIVE PERIPHERAL NERVE INTERFACES (RPNI):," *Plastic and Reconstructive Surgery*, vol. 127, p. 86, May 2011.

[79] D. C. Ursu, M. G. Urbanchek, A. Nedic, P. S. Cederna, and R. B. Gillespie, "In Vivo Characterization of Regenerative Peripheral Nerve Interface Function," *Journal of Neural Engineering*, vol. in press, Jan. 2016.

[80] M. E. Whitcomb, "More on competency-based education," *Academic Medicine: Journal of the Association of American Medical Colleges*, vol. 79, pp. 493–494, June 2004.

[81] H. T. Debas, B. L. Bass, M. F. Brennan, T. C. Flynn, J. R. Folse, J. A. Freischlag, P. Friedmann, L. J. Greenfield, R. S. Jones, F. R. Lewis, M. A. Malangoni, C. A. Pellegrini, E. A. Rose, A. K. Sachdeva, G. F. Sheldon, P. L. Turner, A. L. Warshaw, R. E. Welling, M. J. Zinner, and American Surgical Association Blue Ribbon Committee, "American Surgical Association Blue Ribbon Committee Report on Surgical Education: 2004," *Annals of Surgery*, vol. 241, pp. 1–8, Jan. 2005.

[82] R. K. Reznick and H. MacRae, "Teaching surgical skills–changes in the wind," *The New England Journal of Medicine*, vol. 355, pp. 2664–2669, Dec. 2006.

[83] K. A. Ericsson, "An expert-performance perspective of research on medical expertise: the study of clinical performance," *Medical Education*, vol. 41, pp. 1124–1130, Dec. 2007.

[84] K. A. Ericsson, "Deliberate practice and the acquisition and maintenance of expert performance in medicine and related domains," *Academic Medicine: Journal of the Association of American Medical Colleges*, vol. 79, pp. S70–81, Oct. 2004.

[85] M. A. Memon, D. Brigden, M. S. Subramanya, and B. Memon, "Assessing the surgeon's technical skills: analysis of the available tools," *Academic Medicine: Journal of the Association of American Medical Colleges*, vol. 85, pp. 869–880, May 2010.

[86] K. A. Ericsson, "Deliberate practice and acquisition of expert performance: a general overview," *Academic Emergency Medicine: Official Journal of the Society for Academic Emergency Medicine*, vol. 15, pp. 988–994, Nov. 2008.

[87] J. Chikwe, A. C. de Souza, and J. R. Pepper, "No time to train the surgeons," *BMJ (Clinical research ed.)*, vol. 328, pp. 418–419, Feb. 2004.

[88] C. Carraccio, S. D. Wolfsthal, R. Englander, K. Ferentz, and C. Martin, "Shifting paradigms: from Flexner to competencies," *Academic Medicine: Journal of the Association of American Medical Colleges*, vol. 77, pp. 361–367, May 2002.

[89] N. I. Bhatti and C. W. Cummings, "Competency in surgical residency training: defining and raising the bar," *Academic Medicine: Journal of the Association of American Medical Colleges*, vol. 82, pp. 569–573, June 2007.

[90] R. Brydges, A. Kurahashi, V. Brümmer, L. Satterthwaite, R. Classen, and A. Dubrowski, "Developing criteria for proficiency-based training of surgical technical skills using simulation: changes in performances as a function of training year," *Journal of the American College of Surgeons*, vol. 206, pp. 205–211, Feb. 2008.

[91] C. D. Klink, M. Binnebösel, H. P. Alizai, A. Lambertz, K. T. vonTrotha, E. Junker, C. Disselhorst-Klug, U. P. Neumann, and U. Klinge, "Tension of knotted surgical sutures shows tissue specific rapid loss in a rodent model," *BMC Surgery*, vol. 11, no. 1, p. 36, 2011.

[92] N. H. McKee and W. M. Kuzon, "Functioning free muscle transplantation: making it work? What is known?," *Annals of Plastic Surgery*, vol. 23, pp. 249–254, Sept. 1989.

[93] J. Kobayashi, S. E. Mackinnon, O. Watanabe, D. J. Ball, X. M. Gu, D. A. Hunter, and W. M. Kuzon, "The effect of duration of muscle denervation on functional recovery in the rat model," *Muscle & Nerve*, vol. 20, pp. 858–866, July 1997.

[94] K. Yoshimura, H. Asato, P. S. Cederna, M. G. Urbanchek, and W. M. Kuzon, "The effect of reinnervation on force production and power output in skeletal muscle," *The Journal of Surgical Research*, vol. 81, pp. 201–208, Feb. 1999.

[95] K. Yoshimura, H. Asato, S. S. Jejurikar, P. S. Cederna, M. G. Urbanchek, and W. M. Kuzon, "The effect of two episodes of denervation and reinnervation on skeletal muscle contractile function," *Plastic and Reconstructive Surgery*, vol. 109, pp. 212–219, Jan. 2002.

[96] S. C. Lien, P. S. Cederna, and W. M. Kuzon, "Optimizing skeletal muscle reinnervation with nerve transfer," *Hand Clinics*, vol. 24, pp. 445–454, vii, Nov. 2008.

[97] S. Sunderland, *Nerves and nerve injuries*. Edinburgh ; New York : New York: Churchill Livingstone ; distributed by Longman, 2d ed ed., 1978.

[98] M. E. Jabaley, W. H. Wallace, and F. R. Heckler, "Internal topography of major nerves of the forearm and hand: a current view," *The Journal of Hand Surgery*, vol. 5, pp. 1–18, Jan. 1980.

[99] J. D. Stewart, "Peripheral nerve fascicles: anatomy and clinical relevance," *Muscle & Nerve*, vol. 28, pp. 525–541, Nov. 2003.

[100] G. E. P. Box, "Science and Statistics," *Journal of the American Statistical Association*, vol. 71, pp. 791–799, Dec. 1976.